Flinders
UNIVERSITY

Methyl rotor dependent vibrational interactions in toluene

Jason R. Gascooke and Warren D. Lawrance

Citation: J. Chem. Phys. **138**, 134302 (2013); doi: 10.1063/1.4795439
View online: http://dx.doi.org/10.1063/1.4795439
View Table of Contents: http://jcp.aip.org/resource/1/JCPSA6/v138/i13
Published by the American Institute of Physics.

Methyl rotor dependent vibrational interactions in toluene

Jason R. Gascooke and Warren D. Lawrance[a)]
School of Chemical and Physical Sciences, Flinders University, GPO Box 2100, Adelaide SA 5001, Australia

(Received 22 December 2012; accepted 7 February 2013; published online 2 April 2013)

The methyl rotor dependence of a three state Fermi resonance in S_1 toluene at ~460 cm^{-1} has been investigated using two-dimensional laser induced fluorescence. An earlier time-resolved study has shown the Fermi resonance levels to have different energy spacings at the two lowest methyl rotor states, $m = 0$ and 1 [J. A. Davies, A. M. Green, and K. L. Reid, Phys. Chem. Chem. Phys. **12**, 9872 (2010)]. The overlapped $m = 0$ and 1 spectral features have been separated to provide direct spectral evidence for the m dependence of the resonance. The resonance has been probed at $m = 3a_1'$ for the first time and found to be absent, providing further evidence for a large change in the interaction with m. Deperturbing the resonance at $m = 0$ and 1 reveals that the m dependence arises through differences in the separations of the "zero-order," locally coupled states. It is shown that this is the result of the local "zero-order" states being perturbed by long-range torsion-vibration coupling that shifts their energy by small amounts. The m dependence of the shifts arises from the $\Delta m = \pm 3n$ ($n = 1, 2, \ldots$) coupling selection rule associated with torsion-rotation coupling in combination with the m^2 scaling of the rotor energies, which changes the ΔE for the interaction for each m. There is also an increase in the number of states that can couple to $m = 1$ compared with $m = 0$. Consideration of the magnitude of reported torsion-rotation coupling constants suggests that this effect is likely to be pervasive in molecules with methyl rotors. © *2013 American Institute of Physics*. [http://dx.doi.org/10.1063/1.4795439]

I. INTRODUCTION

Anharmonicity plays an important role in the time dependent redistribution of vibrational energy within polyatomic molecules through the role of anharmonic coupling in mixing vibrational states. It is, however, only one of several mechanisms. Early in the investigation of intramolecular vibrational energy redistribution (IVR) it was realized that the presence of a methyl rotor significantly enhances the process.[1] For example, there is an increase in IVR rate by two orders of magnitude in *p*-fluorotoluene (*p*FT) compared with *p*-difluorobenzene (*p*DFB) at similar vibrational energies.[1–6] In order to provide a detailed understanding of the mechanisms leading to this effect, Reid and co-workers have developed the technique of picosecond time resolved photoelectron spectroscopy as a probe of the behavior of relatively low-lying vibrational levels, with particular application to toluene and *p*FT.[7–14] The aim of the experiments has been to investigate couplings where there are comparatively few potential interactions, allowing the mechanism involved to be deduced.

In this context, Davies *et al.* recently reported a re-investigation of the Fermi resonance occurring at ~460 cm^{-1} in S_1 toluene,[7] which followed earlier work by this group.[13] This resonance occurs at quite low vibrational energy and so is in a very sparse region of the vibrational manifold. It was observed and assigned in earlier spectroscopic work as a two state system,[15] however, the new time-resolved study showed the involvement of a third level. Interestingly, the time-dependent experiments revealed that the spacings between the molecular states are different depending on the excitation of the methyl rotor. Specifically, the experiments probed the time behavior of the Fermi resonance for the $m = 0$ and $m = 1$ methyl rotor levels (m is the quantum number denoting the methyl rotor angular momentum). The observation of an m dependence to the time behavior associated with the Fermi resonance is remarkable since anharmonic coupling is responsible for this mixing and it involves no m-dependent terms. It would be expected that the rotor levels associated with each vibrational state stack up essentially the same and the Fermi resonance interaction would be equivalent at each m. There is currently no explanation for the m dependence of the Fermi resonance. Interestingly, similar differences between $m = 0$ and 1 molecular states have been observed in other cases and it appears to be the rule rather than the exception.[14] Consequently, understanding the origin of the effect in toluene is likely to have wider ramifications.

We have undertaken a spectroscopic investigation of this Fermi resonance in toluene to try to identify the mechanism underlying the m-dependent effect. The key to unraveling the interaction is the ability to detect the states involved in the Fermi resonance with individual m state resolution. Our investigation is based on the technique of two-dimensional laser induced fluorescence (2D-LIF).[16–25] This technique involves measuring a region of the dispersed fluorescence spectrum as the laser is scanned over absorption features. The dispersed fluorescence effectively provides a filter that allows different species to be separated. By focusing on certain spectral features, the LIF spectrum for a particular species can be extracted. In the toluene case, while the $\Delta m = 0$ transitions are significantly overlapped (the m_0^0 and m_1^1 transitions

a)Author to whom correspondence should be addressed. Electronic mail: warren.lawrance@flinders.edu.au.

are observed to be separated by 0.22 cm^{-1}),[26] we demonstrate that the LIF spectrum associated with m_0^0 transitions can be observed separately from the LIF spectrum associated with m_1^1 transitions by monitoring the weak $\Delta m \neq 0$ transitions in dispersed fluorescence. Our analysis has been aided by the recent resonance enhanced multiphoton ionization (REMPI) and zero kinetic energy photoelectron (ZEKE) study of toluene by Gardner *et al.*[27]

II. EXPERIMENTAL DETAILS

Our experimental setup for 2D-LIF has been given in detail previously.[16] The salient features for the present experiments are as follows. The frequency doubled output of a Nd:YAG pumped dye laser (Continuum Surelite-II pumping a Lambda Physik Scanmate operating with Coumarin 503 laser dye; 0.3 cm^{-1} doubled line width; 10 Hz repetition rate) is passed vertically through a stainless steel chamber containing the source, the vertical propagation matching the vertical entrance slit of the spectrometer. The laser beam intersects a horizontal supersonic free jet expansion of 1% toluene in Ar at X/D $\sim$ 10. The resulting fluorescence is dispersed using a home-built spectrometer with a dispersion of $\sim$5 cm^{-1} per mm in the wavelength region of the present experiments. The dispersed fluorescence is detected with a 25 mm diameter gated image intensifier with single photon detection sensitivity. The loss of sensitivity at the edges (due to the image intensifier vertical dimension no longer matching the slit height) leads to the effective width of the region viewed being $\sim$80–100 cm^{-1}. The image intensifier is gated to detect fluorescence in a time window near the laser; for the experiments described herein, it was gated to open post the laser pulse to minimise the detection of scattered laser light. The image intensifier output at each laser shot is captured using a charge coupled device (CCD) camera. The CCD image is downloaded to a computer and analysed to identify and record the centre of each spot observed and a histogram of events at each camera pixel position is built up. The process continues for a preset number of laser shots with the laser fixed in wavelength, producing a section of the dispersed fluorescence spectrum at that laser wavelength. The laser then steps to the next wavelength and the process repeats until the laser has scanned the region required. The result is a three-dimensional surface of fluorescence intensity as a function of both the laser and dispersed fluorescence wavelengths. We refer to this surface as a 2D-LIF spectral image.

Absolute transition energies are estimated to be accurate to $\pm$0.1 cm^{-1}. Comparison of several repeat images suggests that the separations between features on an image are accurate to within 0.02 cm^{-1} on the laser axis and 0.05 cm^{-1} on the fluorescence axis. Bands are measured at the minimum in their rotational contour.

III. RESULTS

A. Vibrational mode numbering

Several mode numbering schemes have been used for assigning the vibrations of toluene.[15,28–32] The situation is summarized in Appendix A, which also provides the rationale for the numbering scheme used here. It is based on the scheme for monosubstituted benzene derivatives proposed by Gardner and Wright,[33] extended to account for the methyl modes. Table I gives the S_0 vibrational frequencies and correlates the various mode numbering schemes that have been used.

In our earlier spectroscopic investigation of S_1 toluene we assigned the Fermi resonance to an interaction between (in Gardner and Wright's numbering scheme) 11^1 and 19^120^1, with 11^1 carrying the oscillator strength.[15] The study by Davies *et al.* indicated the involvement of a third state, 14^2 (Ref. 7). Davies *et al.* used the Wilson notation, and hence labeled the interaction as involving $6a^1$ (11^1), $10b^116b^1$ (19^120^1), and $16a^2$ (14^2).

B. Methyl rotor overview

Before presenting the results, we provide a synopsis of the spectroscopy of toluene with respect to its methyl rotor levels. The calculation of the methyl rotor levels is well summarised in the review article by Spangler[34] and papers from Weisshaar's group.[35–39] The free rotor has energies $E = m^2F$, where F is the internal rotation constant associated with the methyl rotation and the quantum number m takes values of 0, $\pm$1, $\pm$2, ... The positive and negative m values correspond to the methyl group spinning in opposite directions. The free rotor basis states are $\psi = \exp(im\phi)$, where ϕ is the angle of rotation of the methyl group. The methyl rotor in toluene is not free but involves a six-fold potential, i.e., a $\frac{V_6}{2}(1 - \cos 6\phi)$ term, where V_6 denotes the barrier height. Its energies are calculated as the eigenvalues of the Hamiltonian matrix constructed in the free rotor basis. The V_6 potential couples the free rotor states differing in m by $\pm$6 with a coupling term of $-V_6/4$. The most significant effect of this barrier is to directly couple the degenerate $m = \pm 3$ states. This causes them to split apart to form two levels, the symmetric and anti-symmetric combinations of the $m = \pm 3$ basis functions, which are separated by $V_6/2$.

Breen *et al.* reported rotor-resolved LIF and dispersed fluorescence spectra of toluene in the region of the 0_0^0 band, providing values for V_6 and F in the ground and excited electronic states.[40] Their spectra were consistent with $V_6 = -25$ cm^{-1} in S_1 and -5 cm^{-1} in S_0, with $F = 5.2$ cm^{-1} in both states. The negative sign for V_6 indicates that the minimum involves the staggered position where one of the methyl C–H bonds is at 90° to the aromatic plane. These S_0 values are broadly consistent with earlier, more precise microwave studies which gave $|V_6| = 4.876$ cm^{-1} and $F = 5.436$ cm^{-1} (Refs. 41–43). An electronic spectrum showing rotational structure was first reported by East *et al.*[44] A subsequent higher resolution study by Borst and Pratt reported the rotational structure of the 0_0^0 band, giving more precise V_6 and F values for the upper state of -26.376 and 5.298 cm^{-1}, respectively,[26] and unambiguously identifying the minimum as the staggered position in both electronic states. Borst and Pratt reported slightly different F values for the $m = 0$, 1, and $3a_1''$ levels in S_1, indicating a non-zero centrifugal distortion term, dF. A value for this term has not been determined in

TABLE I. A comparison of the different nomenclatures and mode numbering schemes used to label the vibrational modes of toluene.

Symmetry G_{12}/C_{2v}	ν (cm^{-1})	Hickman *et al.*[15]	Pitzer and Scott[28]	Fuson *et al.*[29]	Sverdlov *et al.*[31]	Varsanyi[30]	Gardner and Wright[33]	This work
A_1'/A_1	3087	1	20*a*	7*a*	20*a*	20*a*	$\mathcal{M}_1$	$\mathcal{M}_1$
	3063	2	2	20*a*	13	2	$\mathcal{M}_2$	$\mathcal{M}_2$
	3055	3	13	2	7*a*	7*a*	$\mathcal{M}_3$	$\mathcal{M}_3$
	1605	5	8*a*	8*a*	8*a*	8*a*	$\mathcal{M}_4$	$\mathcal{M}_4$
	1494	6	19*a*	19*a*	19*a*	19*a*	$\mathcal{M}_5$	$\mathcal{M}_5$
	1210	8	7*a*	13	2	13	$\mathcal{M}_6$	$\mathcal{M}_6$
	1175	9	9*a*	9*a*	9*a*	9*a*	$\mathcal{M}_7$	$\mathcal{M}_7$
	1030	10	18*a*	18*a*	18*a*	18*a*	$\mathcal{M}_8$	$\mathcal{M}_8$
	1003	11	1	12	12	12	$\mathcal{M}_9$	$\mathcal{M}_9$
	785	12	12	1	1	1	$\mathcal{M}_{10}$	$\mathcal{M}_{10}$
	521	13	6*a*	6*a*	6*a*	6*a*	$\mathcal{M}_{11}$	$\mathcal{M}_{11}$
	2921	4	*M*1	ν_s	...	ν_s	...	$\mathcal{S}_1$
	1379	7	*M*3	δ_s	...	δ_s	...	$\mathcal{S}_2$
A_2'/A_2	964	14	17*a*	17*a*	17*a*	17*a*	$\mathcal{M}_{12}$	$\mathcal{M}_{12}$
	843	15	10*a*	10*a*	10*a*	10*a*	$\mathcal{M}_{13}$	$\mathcal{M}_{13}$
	407	16	16*a*	16*a*	16*a*	16*a*	$\mathcal{M}_{14}$	$\mathcal{M}_{14}$
A_1''/B_2	3039	26	20*b*	7*b*	20*b*	7*b*	$\mathcal{M}_{21}$	$\mathcal{M}_{21}$
	3029	27	7*b*	20*b*	7*b*	20*b*	$\mathcal{M}_{22}$	$\mathcal{M}_{22}$
	1586	29	8*b*	8*b*	8*b*	8*b*	$\mathcal{M}_{23}$	$\mathcal{M}_{23}$
	1445	31	...	19*b*	19*b*	19*b*	$\mathcal{M}_{24}$	$\mathcal{M}_{24}$
	1312	32	19*b*	3	14	14	$\mathcal{M}_{25}$	$\mathcal{M}_{25}$
	1280	33	3	...	3	...	$\mathcal{M}_{26}$	$\mathcal{M}_{26}$
	1155	34	9*b*	9*b*	9*b*	9*b*	$\mathcal{M}_{27}$	$\mathcal{M}_{27}$
	1080	35	15	18*b*	18*b*	18*b*	$\mathcal{M}_{28}$	$\mathcal{M}_{28}$
	623	37	6*b*	6*b*	6*b*	6*b*	$\mathcal{M}_{29}$	$\mathcal{M}_{29}$
	342	38	18*b*	15	15	15	$\mathcal{M}_{30}$	$\mathcal{M}_{30}$
	2952	28	*M*2	ν_a'	...	ν_{as}	...	$\mathcal{S}_3$
	1463	30	*M*4	δ_a'	...	δ_{as}^+	...	$\mathcal{S}_4$
	1040	36	*M*6	r'	...	δ_{as}^-	...	$\mathcal{S}_5$
A_2''/B_1	978	20	5	5	5	5	$\mathcal{M}_{15}$	$\mathcal{M}_{15}$
	895	21	17*b*	17*b*	17*b*	17*b*	$\mathcal{M}_{16}$	$\mathcal{M}_{16}$
	728	22	10*b*	11	10*b*	11	$\mathcal{M}_{17}$	$\mathcal{M}_{17}$
	695	23	4	4	4	4	$\mathcal{M}_{18}$	$\mathcal{M}_{18}$
	464	24	16*b*	16*b*	11	16*b*	$\mathcal{M}_{19}$	$\mathcal{M}_{19}$
	216	25	11	10*b*	16*b*	10*b*	$\mathcal{M}_{20}$	$\mathcal{M}_{20}$
	2979	17	*M*2	ν_a''	...	ν_{as}	...	$\mathcal{S}_6$
	1450	18	*M*4	δ_a''	...	δ_{as}^+	...	$\mathcal{S}_7$
	1040	19	*M*6	r''	...	δ_{as}^-	...	$\mathcal{S}_8$

S_0 because the higher m states have not been measured with sufficient accuracy. Since the constants are known, the m state energies in both 0_0 and 0^0 can be calculated with reasonable precision.[34] Table II shows the methyl rotor energy levels up to $m = 4$ predicted based on the constants determined in the high resolution studies. The states are labeled according to the G_{12} symmetry elements.[34,40]

Throughout this paper transitions involving m will be labeled using the usual spectroscopic convention m_a^b, where a indicates the value of m in the S_0 state and b is its value in S_1. For the degenerate $m = \pm1, \pm2, \pm4 \ldots$, states the unsigned m value is used, however, for $m = \pm3, \pm6, \ldots$, the degeneracy is lifted by the V_6 term and two non-degenerate m states are formed that are symmetric and anti-symmetric linear combinations of the $\psi = \exp(im\phi)$ basis states. To identify these using the m_a^b notion, we use a trailing (+) to indicate the symmetric combination and a (−) to indicate the anti-symmetric one. For example, the $3a_1''$ state is the symmetric combination (see Table II) and the absorption transition $m'' = 0 \rightarrow m' = 3a_1''$ is written $m_0^{3(+)}$. For rotor transitions accompanying

TABLE II. The calculated methyl rotor levels in 0_0 and 0^0 toluene based on the constants determined in high resolution studies.

m[a]	Symmetry	S_0 Energy[b] (cm^{-1})	S_1 Energy[c] (cm^{-1})
0	a'_1	0	0
1	e''	5.43	5.23
2	e'	21.73	20.70
3(−)	a_2''	47.72	40.79
3(+)	a_1''	50.15	53.97
4	e'	87.01	83.78

[a](+) indicates the symmetric combination of basis functions for this m; (−) indicates the anti-symmetric combination.
[b]$V_6 = -4.874\ cm^{-1}$; $F = 5.436\ cm^{-1}$ (Refs. 41–43).
[c]$V_6 = -26.376\ cm^{-1}$; $F = 5.298\ cm^{-1}$; $dF = 0.008\ cm^{-1}$ (Ref. 26).

the 0_0^0 transition, the 0_0^0 change is omitted, e.g., the transition is written $m_0^{3(+)}$ rather than $0_0^0 m_0^{3(+)}$.

The $m = 3n$ and $m = 3n \pm 1$ states ($n = 0, 1, 2, \ldots$) belong to different nuclear spin states and, since collisional cooling during the supersonic expansion does not change nuclear spin, the m state population collapses to be in $m = 0$ and $m = 1$ (Ref. 40). The changes in m that occur in transitions between the ground and excited electronic states cannot lead to a change in nuclear spin. The dominant transitions are those involving $\Delta m = 0$ but weak $\Delta m \neq 0$ transitions are also seen.[40] For toluene, the $\Delta m = 3$ absorption transition $m_0^{3(+)}$ has been observed,[26,40] while the $m_0^{3(-)}$ transition is symmetry forbidden[40] and has not been reported. The absorption transitions m_1^2, m_1^4, and m_1^5 have also been reported, as have the fluorescence transitions $m_{3(+)}^0$ and m_2^1, m_4^1, and m_5^1 (Ref. 40). It can be seen from Table II that the $\Delta m = 0$ transitions from $m'' = 0$ and 1 are strongly overlapped: the calculated separation is 0.20 cm^{-1}, which compares well with the observed value of 0.22 cm^{-1} (Ref. 26). Here, we have introduced the notation of a double prime on the m to indicate the S_0 state; a single prime will be used to indicate the S_1 state.

The 2D-LIF images are presented with the laser wavenumber along the x-axis and the fluorescence wavenumber along the y-axis. Features are labelled by their (x,y) value, i.e., the (absorption, emission) wavenumber values. The methyl rotor absorption transitions will be seen in fluorescence via the $\Delta m = 0$ transition since this is by far the strongest band.[34,40,45] For example, the m_1^2 absorption transition would be observed via the m_2^2 emission band, leading to a feature in the 2D-LIF image at (m_1^2,m_2^2). Because the methyl rotor energies are similar in the S_0 and S_1 states (see Table II), the $\Delta m = 0$ rotor transitions occur at similar energies. For this reason, excitation to a series of S_1 rotor levels leads to a series of transitions that appear at approximately the same emission wavenumber but different absorption wavenumbers. This leads to features in the 2D-LIF spectral image that are near-horizontal with the non-rotor transition on which they are built. This is analogous to the previously reported situation for observing absorption transitions associated with van der Waals modes.[17] The rotor energies in both S_1 and S_0 can be determined from the positions of these features in the 2D-LIF spectral image. The S_0 rotor energies can also be observed via weak $\Delta m \neq 0$ emission features.

C. 0^0 region

Prior to examining the 11^1 Fermi resonance region, we establish the features expected in the 2D-LIF spectral images by investigating the 0_0^0 band region of toluene, where perturbations are minimized. The 2D-LIF spectral image of this region is shown in Fig. 1(a). Toluene features are assigned in the figure. The LIF spectrum, extracted by vertical integration of a horizontal slice encompassing the $\Delta m = 0$ emission features, is shown in Fig. 1(b). Features involving $\Delta m \neq 0$ changes have extended and unusual shapes. Determining the band origin in these cases generally requires that the rotational features be simulated. A detailed analysis of the methyl rotor bands will be provided in a forthcoming publication. We note the weak feature observed in the image at (37 517 cm^{-1}, 37 471 cm^{-1}), which we assign to absorption via the $m_0^{3(-)}$ transition followed by emission $m_{3(-)}^{3(-)}$. Absorption from $m'' = 0$ to $m' = 3a_2''$ is forbidden but analogous transitions have been observed in related systems where it has been argued that they arise due to torsion-rotation coupling.[37,38]

The image reveals several key features to unraveling the m dependence of the Fermi resonance. Although they are weak, the $\Delta m \neq 0$ transitions are clearly seen both in absorption from m_0 and m_1 (the horizontal series of bands at the top of the figure) and emission from m^0 and m^1 (the vertical series of bands at the left hand side of the figure). Thus, while the m_0^0 and m_1^1 absorption and emission bands strongly overlap, the $m_{3(+)}^0$, m_2^1, and m_4^1 emission bands provide windows for viewing the absorption transitions to $m' = 0$ and $m' = 1$ separately. This is illustrated in Fig. 2(a) where the LIF spectra associated with the m_0^0 and m_1^1 absorption transitions are displayed individually. The m_0^0 spectrum is extracted by integrating vertically over the $m_{3(+)}^0$ 2D-LIF feature, while the m_1^1 spectrum is extracted by integrating vertically over the m_4^1 spectral feature. Combining this ability to observe m^0 and m^1 levels separately with observation of the absorption bands m_1^2, $m_0^{3(+)}$, and m_1^4 suggests that it may be possible to probe the $11^1-19^120^1-14^2$ Fermi resonance at $m' = 0-4$, although the weak, broad rotational structure seen in the m_1^2 and m_1^4 bands may make the resonance problematic to observe for $m' = 2$ and 4.

The remaining features in the image belong to a weak series of bands that extends horizontally across the image at an emission wavenumber of ~37 450 cm^{-1}. These are due to the toluene-Ar van der Waals complex[46–48] and are discussed in a separate publication.[49]

D. 11^1 Fermi resonance region

1. Overview spectral image

Figure 3 shows the 2D-LIF spectral image for the $(11_0^1, 11_1^1)$ and the surrounding rotor transition region. The region shown in this figure is analogous to that shown in Fig. 1 for the $(0_0^0,0_0^0)$ and associated rotor transitions. The 11_0^1 band is not very intense relative to the 0_0^0 band[15] and the signal level of the spectral image in Fig. 3 is considerably reduced compared with that seen in Fig. 1. Nevertheless, the Fermi resonance is clearly visible as two intense features in the top left hand corner of the image where the single $(11_0^1, 11_1^1)$ feature would otherwise be seen. A very weak third feature can be just made out to the lower left of the stronger Fermi resonance feature. Ignoring the mixing due to the Fermi resonance, these three features are labeled in order of increasing laser excitation energy as $(14_0^2, 14_2^2)$, $(11_0^1, 11_1^1)$, and $(19_0^120_0^1, 19_1^120_1^1)$, respectively. It is clear that the features associated with the perturbed 11^1 and 19^120^1 levels are significantly more intense than the very weak feature associated with 14^2. It is important to recognise that since the relative intensities seen in the images are a product of the intensities for both the excitation and emission transitions involved, they differ from those usually associated with LIF or REMPI spectra. In the context of

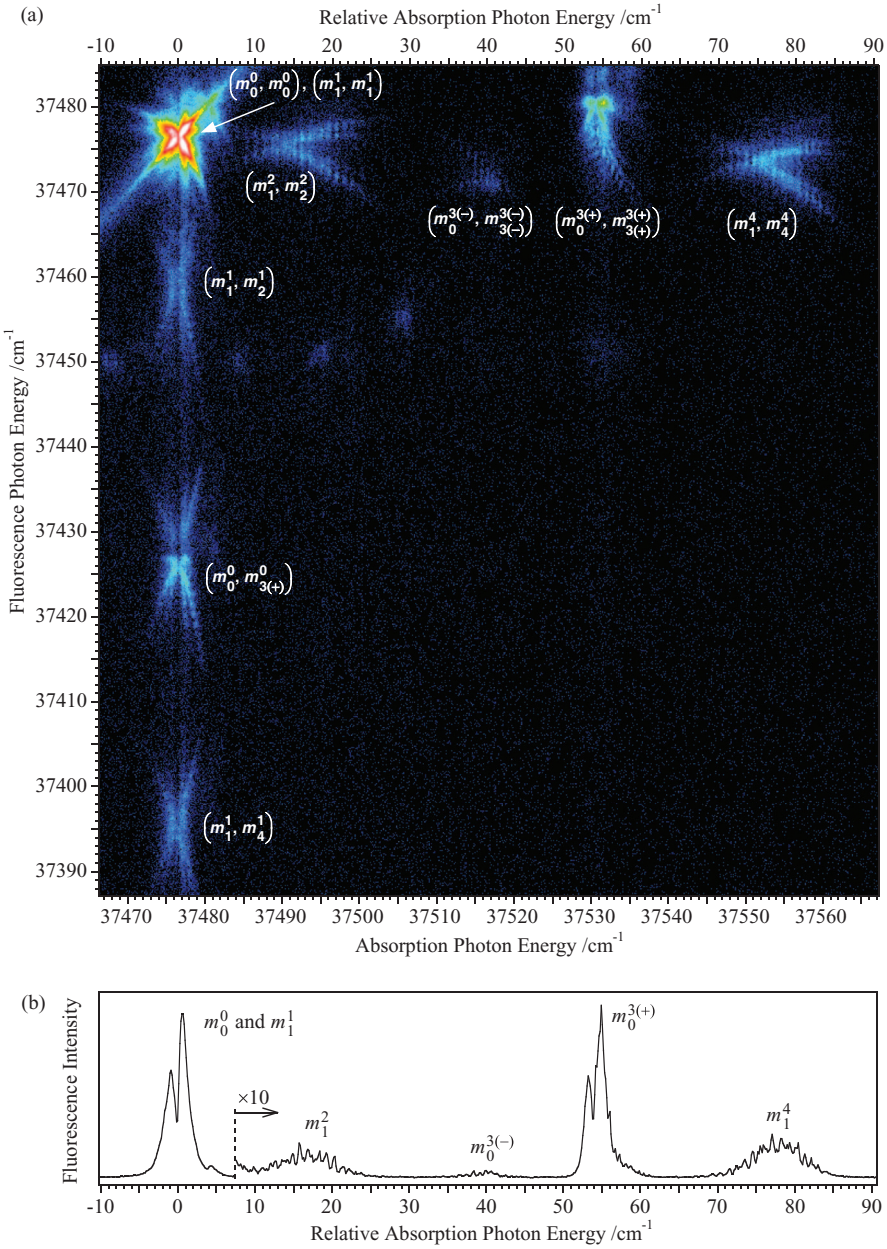

FIG. 1. (a) A 2D-LIF spectral image near the $(0_0^0,0_0^0)$ band region of toluene. The series of horizontal features at the top of the image are associated with absorption from $m'' = 0$ and 1 to various methyl rotor states in S_1. The series of vertical features on the left of the image are associated with emission from $m' = 0$ and 1 to various methyl rotor states in S_0. The weak sequence of horizontal features near 37 450 cm^{-1} is due to transitions of the toluene-Ar van der Waals complex (Ref. 49). Assignments for the toluene features are given in the figure. The horizontal axis at the top of the figure shows the displacement relative to the m_0^0 band at 37 476.6 cm^{-1} (Ref. 26). (b) The LIF spectrum extracted from (a) by vertical integration of a horizontal slice encompassing the $\Delta m = 0$ emission features. The horizontal slice covered the emission region 37 467 to 37 485 cm^{-1}. The small peak at +4.3 cm^{-1} is due to ^{13}C isotopomers in natural abundance (Ref. 18).

the Fermi resonance, the relative intensities are sensitive to the particular emission transition monitored, as will be shown below.

The spectral image (Fig. 3) indicates that each of the Fermi resonance features is duplicated and instead of a single cross appears as two crosses slightly shifted. This separation is associated with the $m = 0$ and $m = 1$ rotor levels for these vibrations and is examined in detail in Sec. IV.

As discussed when presenting the 0_0^0 region image, the $\Delta m = 0$ absorption features from $m'' = 0$ and $m'' = 1$ are difficult to separate because they overlap, however, the $\Delta m \neq 0$ emission bands such as $11_1^1 m_{3(+)}^0$, $11_1^1 m_2^1$, and $11_1^1 m_4^1$ provide a means to do so. The weak features associated with these emission transitions are seen in the vertical series of features observed below the Fermi resonance bands. Figure 2 shows *m*–resolved LIF profiles for several of the prominent bands. This figure clearly shows a variation in the $m_0^0 - m_1^1$ separation associated with different terminating S_1 vibrations.

In terms of the remaining features, the $(11_0^1 m_0^{3(+)}, 11_1^1 m_{3(+)}^{3(+)})$ band shows that the $11_0^1 m_0^{3(+)}$ absorption band is present but the corresponding features expected from the other levels involved in the Fermi

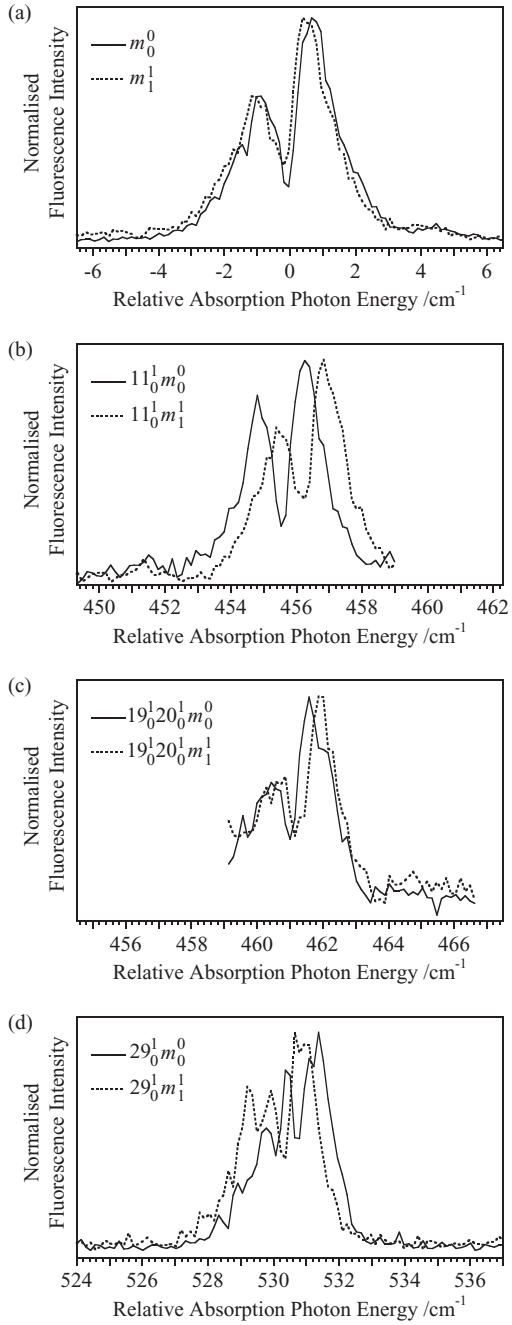

FIG. 2. LIF spectra of the m_0^0 and m_1^1 components associated with (a) 0_0^0, (b) 11_0^1, (c) $19_0^1 20_0^1$, and (d) 29_0^1 absorption transitions. These spectra have been extracted from 2D-LIF spectral images by integrating vertically over the $m_{3(+)}^0$ and m_2^1 emission bands, respectively. The spectra in (a) were extracted from Fig. 1, the spectra in (b) and (c) were extracted from Fig. 4, and the spectra in (d) were extracted from Fig. 3. This illustrates that the $m' = 0$ and $m' = 1$ levels associated with a S_1 vibration can be monitored separately through an appropriate choice of emission wavelengths. The horizontal axis shows the displacement relative to the m_0^0 band at 37 476.6 cm^{-1} (Ref. 26).

resonance are not evident at $m' = 3a_1''$. The $(11_0^1 m_1^2, 11_1^1 m_2^2)$ feature is too weak to be observed while the $(11_0^1 m_1^4, 11_1^1 m_4^4)$ feature is obscured by emission associated with excitation of the 29_0^1 transition, which is responsible for the strong vertical series of bands on the right hand side of the figure. Thus, we are unable to observe the Fermi resonance for $m' = 2$ and 4.

2. Detailed probes of the Fermi resonance

The image shown in Fig. 3 indicates that the $14^2 - 11^1 - 19^1 20^1$ Fermi resonance can be probed in our experiment for the methyl rotor levels $m' = 0$, 1, and $3a_1''$. At $m' = 0$ the resonance is probed by exciting the m_0^0 transitions for the vibrational states involved while monitoring appropriate $m_{3(+)}^0$ transitions in fluorescence. $m' = 1$ is probed in a similar manner, with excitation via m_1^1 transitions and the m_2^1 or m_4^1 transitions monitored in fluorescence. At $m' = 3a_1''$ the resonance is probed by exciting the $m_0^{3(+)}$ transitions and monitoring the associated $m_{3(+)}^{3(+)}$ transitions in fluorescence.

Figure 4 shows a higher sensitivity 2D-LIF spectral image obtained by scanning the laser over the limited region encompassing the absorption features $14_0^2 m_0^0$, $14_0^2 m_1^1$, $11_0^1 m_0^0$, $11_0^1 m_1^1$, $19_0^1 20_0^1 m_0^0$, and $19_0^1 20_0^1 m_1^1$ while monitoring emission from the excited states to $11_1 m_0$, $11_1 m_1$, $11_1 m_2$, $11_1 m_{3(+)}$, and $11_1 m_4$. By virtue of the fluorescence transitions probed, the features seen in Fig. 4 are sensitive to the 11^1 component of the coupled states. Probing on other appropriately chosen fluorescence transitions can highlight the other components. Figures 5 and 6 show the 2D-LIF spectral images obtained by scanning the laser over the same absorption features shown in Fig. 4 but with emission monitored from the excited states to $19_1 20_1 m_0$ and $19_1 20_1 m_1$ (Fig. 5) and $14_2 m_0$ and $14_2 m_1$ (Fig. 6), highlighting the $19^1 20^1$ and 14^2 components, respectively. Comparison of the images shows the significantly different intensity patterns resulting from monitoring the different zero-order components.

Figure 7 shows the 2D-LIF spectral image obtained by scanning the laser over the region where the absorption features $14_0^2 m_0^{3(+)}$, $11_0^1 m_0^{3(+)}$, and $19_0^1 20_0^1 m_0^{3(+)}$ are expected while monitoring emission from the excited states to $11_1 m_{3(+)}$. This reveals the Fermi resonance at $m' = 3a_1''$. It is obvious from the image that the resonance, so prominent at $m' = 0$ and 1, is absent in the image for $m' = 3a_1''$.

The spectral images in Figs. 4–6 have been analysed to determine the relative intensities (Table III) and band separations (Table IV) of the Fermi resonance components at $m' = 0$ and $m' = 1$. We note that the ordering of the $11_0^1 m_0^0$ and $11_0^1 m_1^1$ transition energies is reversed compared to the situation at the 0_0^0 band. An energy level diagram showing the relative energies of the three Fermi resonance coupled states at $m = 0$ and $m = 1$ is shown in Fig. 8. The relative intensities seen in the images differ from those associated with LIF spectra since they are a product of the intensities for both the excitation and emission transitions involved. Tables III and IV show that the relative intensities of the bands are similar at each m, however, the separation of the eigenstates is different. Given that the anharmonic coupling matrix elements for Fermi resonance are independent of m, this indicates a change in the spacings of the zero-order states. This will be discussed in detail in Sec. IV.

An unexpected observation that is seen prominently in Fig. 4 is a doubling of the Fermi resonance features along the dispersed fluorescence axis. It is most clearly evident in the $(11_0^1, 11_1^1)$ case. The doubling indicates a significant increase in the separation between the $(11_0^1 m_0^0, 11_1^1 m_0^0)$ and $(11_0^1 m_1^1, 11_1^1 m_1^1)$ features compared with the situation for 0_0^0.

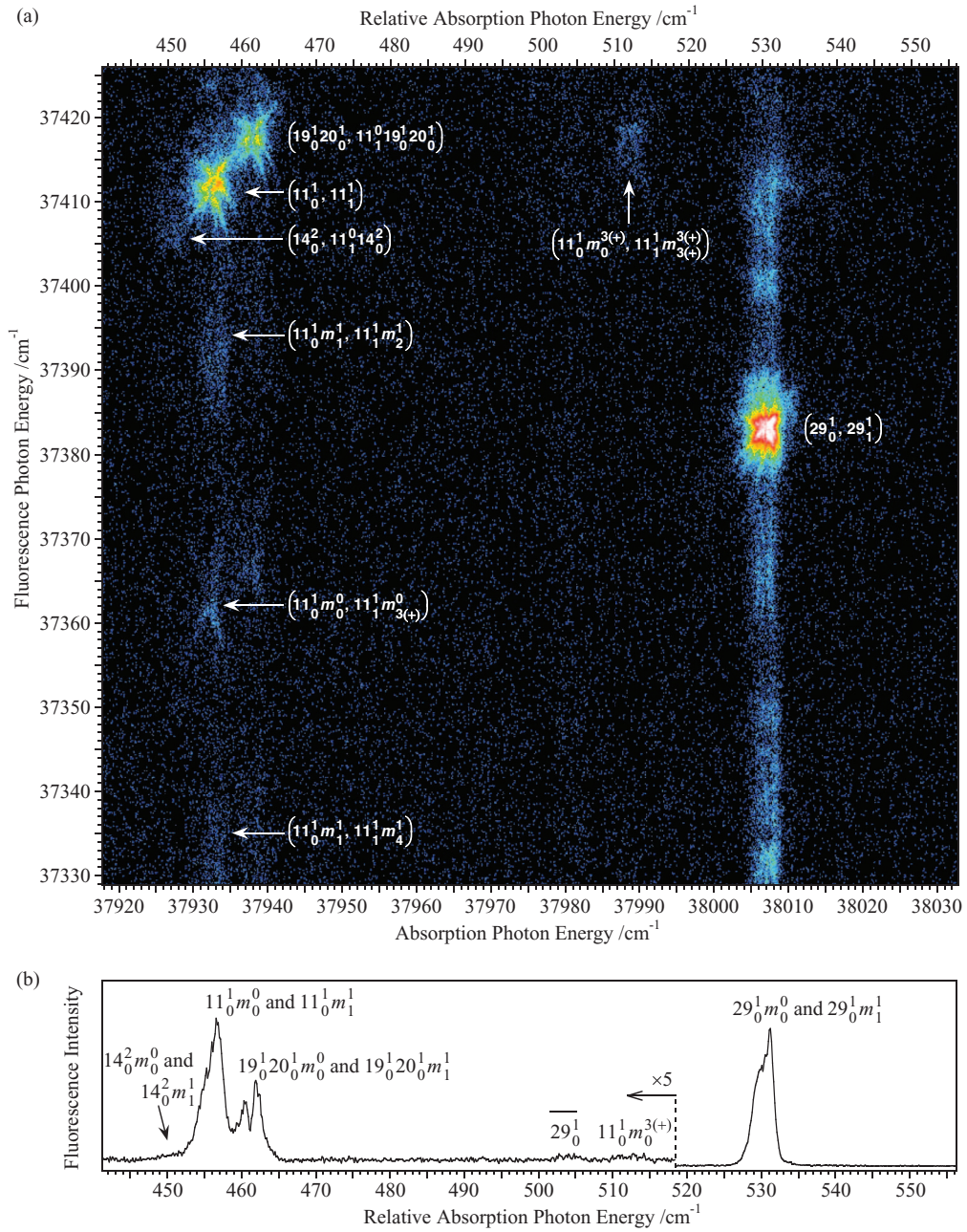

FIG. 3. (a) 2D-LIF spectral image for the $(11_0^1,11_1^1)$ band and associated m transitions. The image is analogous to that shown in Fig. 1 for the $(0_0^0,0_0^0)$ region. The $14^2-11^1-19^120^1$ Fermi resonance is revealed through the two intense features in the top left hand corner of the image where the single $(11_0^1,11_1^1)$ feature would otherwise be seen. The assignments for selected features are displayed in the figure. The $\Delta m = 0$ transitions are omitted from the labels while the $\Delta m \neq 0$ transitions are only labeled for the $(11_0^1,11_1^1)$ features. The horizontal axis at the top of the figure shows the displacement relative to the m_0^0 band at 37 476.6 cm^{-1} (Ref. 26). (b) The LIF spectrum is obtained by vertically integrating the 2D-LIF spectral image.

From Table II, the m_0^0 and m_1^1 transitions are separated by 0.2 cm^{-1}. The images indicate that the separation between the m_0 and m_1 states in the terminating 11_1 level is different from the value in 0_0. The reasons for this change in $m = 0-1$ separation will be discussed in detail in Sec. IV C.

IV. DISCUSSION

The data presented above provide clear evidence that the Fermi resonance involving anharmonic coupling amongst the triad of levels $14^2-11^1-19^120^1$ changes significantly with the methyl torsional level involved. At $m = 0$ and 1 the 11^1 and 19^120^1 states are quite strongly mixed, yet at $m = 3a_1''$ the mixing is so weak that it is not observed. Clearly, the simple notion that the torsional levels add to each of the vibrations to produce a ladder of interacting states that is the same at each m is overly simplistic.

In this section we first deconvolute the Fermi resonance at each m to extract the zero-order states and anharmonic coupling matrix elements. This reveals that the coupling matrix elements are similar in the $m = 0$ and $m = 1$ cases but that the separation between the zero-order levels is different. We then

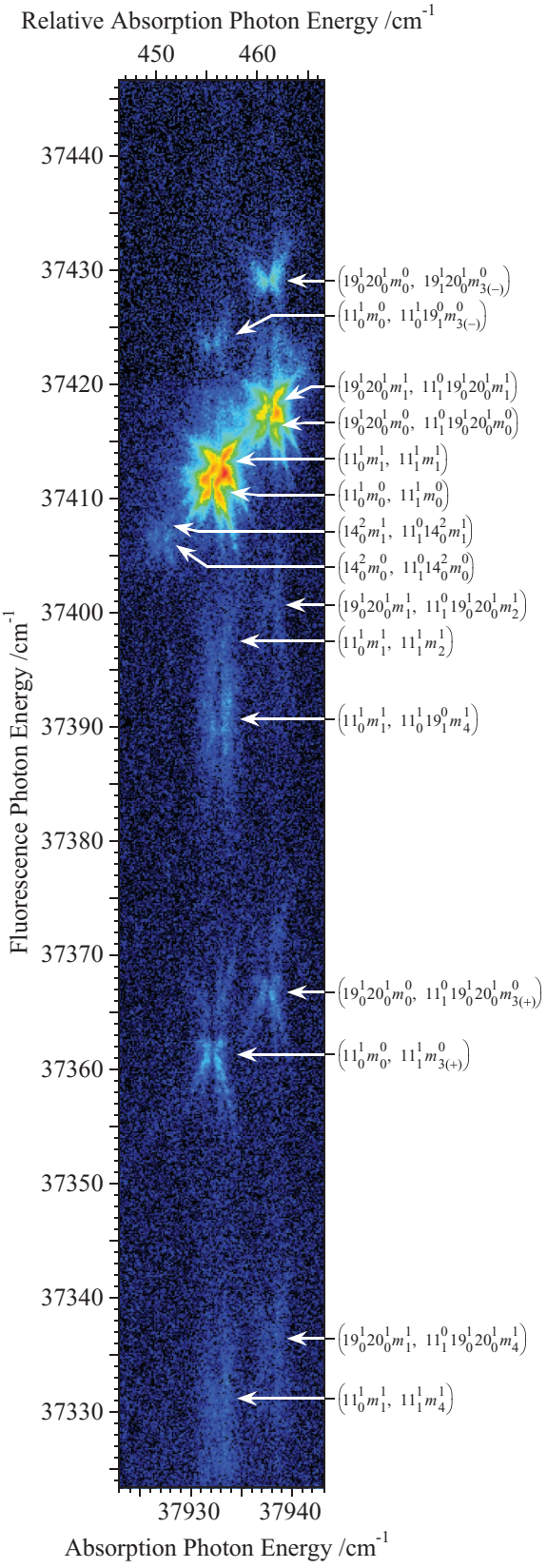

FIG. 4. The 2D-LIF spectral image obtained by scanning the laser over the absorption features $14_0^2 m_0^0$, $14_0^2 m_1^1$, $11_0^1 m_0^0$, $11_0^1 m_1^1$, $19_0^1 20_0^1 m_0^0$, $19_0^1 20_0^1 m_1^1$ while monitoring emission from the excited states to $11_1 m_0$, $11_1 m_1$, $11_1 m_2$, and $11_1 m_{3(+)}$. This image reveals the 11^1 component of the coupled states at $m = 0$ and 1. The horizontal axis at the top of the figure shows the displacement relative to the m_0^0 band at 37 476.6 cm^{-1} (Ref. 26).

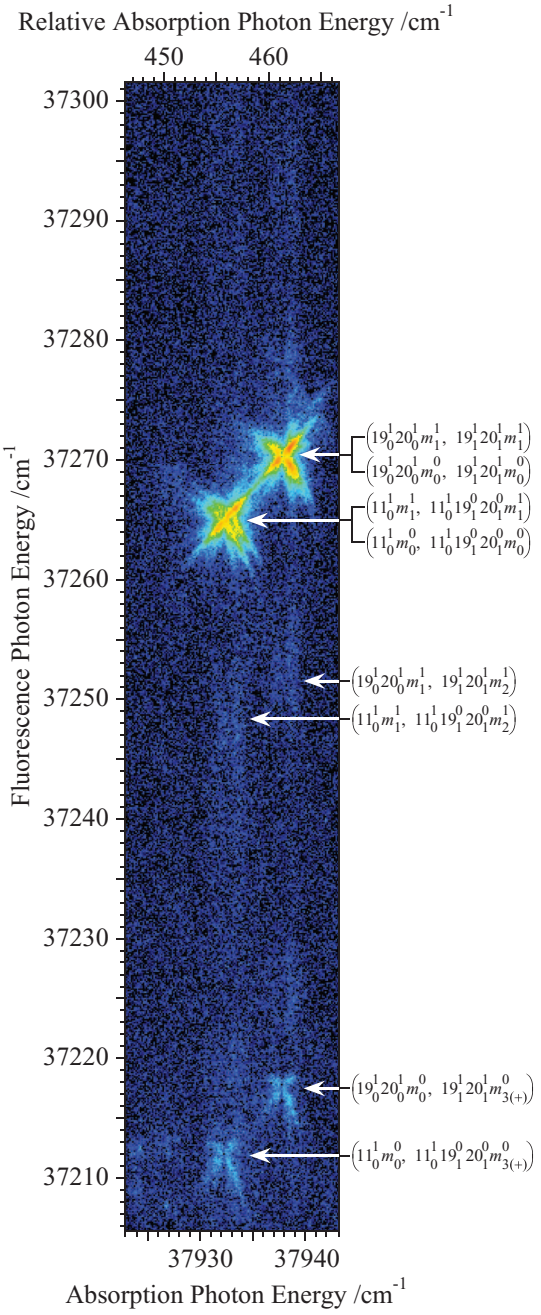

FIG. 5. The 2D-LIF spectral image obtained by scanning the laser over the same absorption features shown in Fig. 4 but with emission monitored to $19_1 20_1 m_0$ and $19_1 20_1 m_1$, revealing the $19^1 20^1$ component in the coupled states. The horizontal axis at the top of the figure shows the displacement relative to the m_0^0 band at 37 476.6 cm^{-1} (Ref. 26).

compare our spectral results with the outcome of the analysis of the quantum beat data obtained by Davies *et al.*[7] Following this we consider the separation of the m levels for 11_1 because it provides a simpler illustration of the effect responsible for the m-dependent shifts seen in the $14^2 - 11^1 - 19^1 20^1$ Fermi resonance. The torsion-vibration state density in the 11_1 region is low, allowing the underlying effect of torsion-vibration coupling to be revealed. Finally, we examine how torsion-vibration coupling can lead to the observed m dependence of the $14^2 - 11^1 - 19^1 20^1$ Fermi resonance and comment

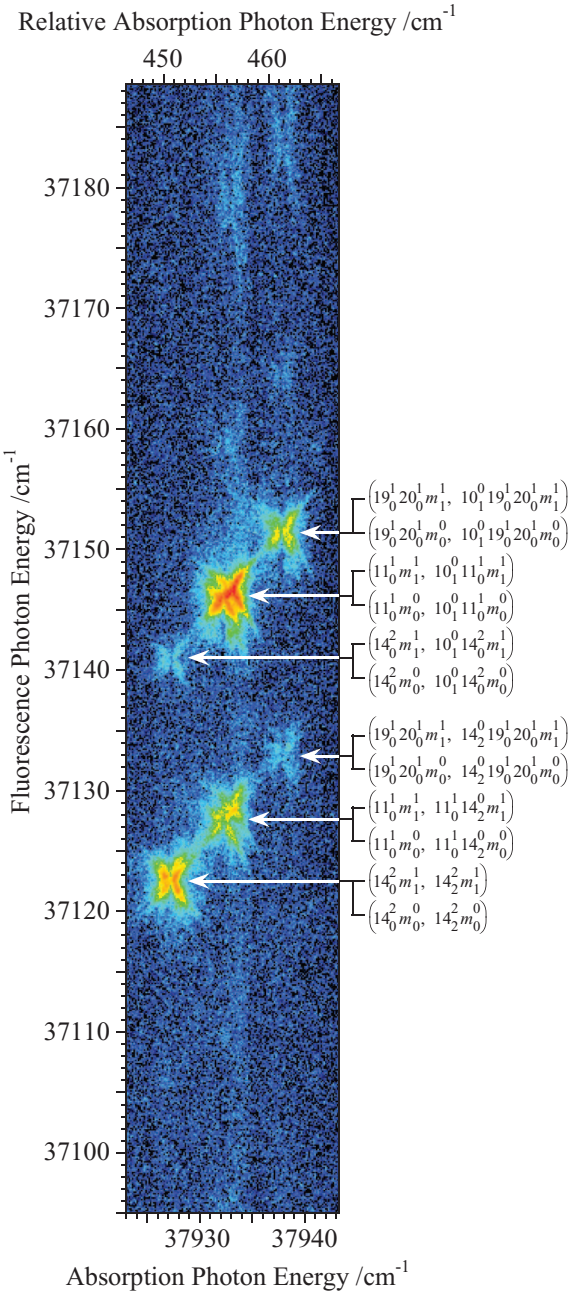

FIG. 6. The 2D-LIF spectral image obtained by scanning the laser over the same absorption features shown in Fig. 4 but emission monitored to $14_2 m_0$ and $14_2 m_1$ (the transitions to $14_2 m_2$ and $14_2 m_{3(+)}$ are too weak to be observed here), revealing the 14^2 component in the coupled states (this is the lower set of features in the figure). The horizontal axis at the top of the figure shows the displacement relative to the m_0^0 band at 37 476.6 cm^{-1} (Ref. 26).

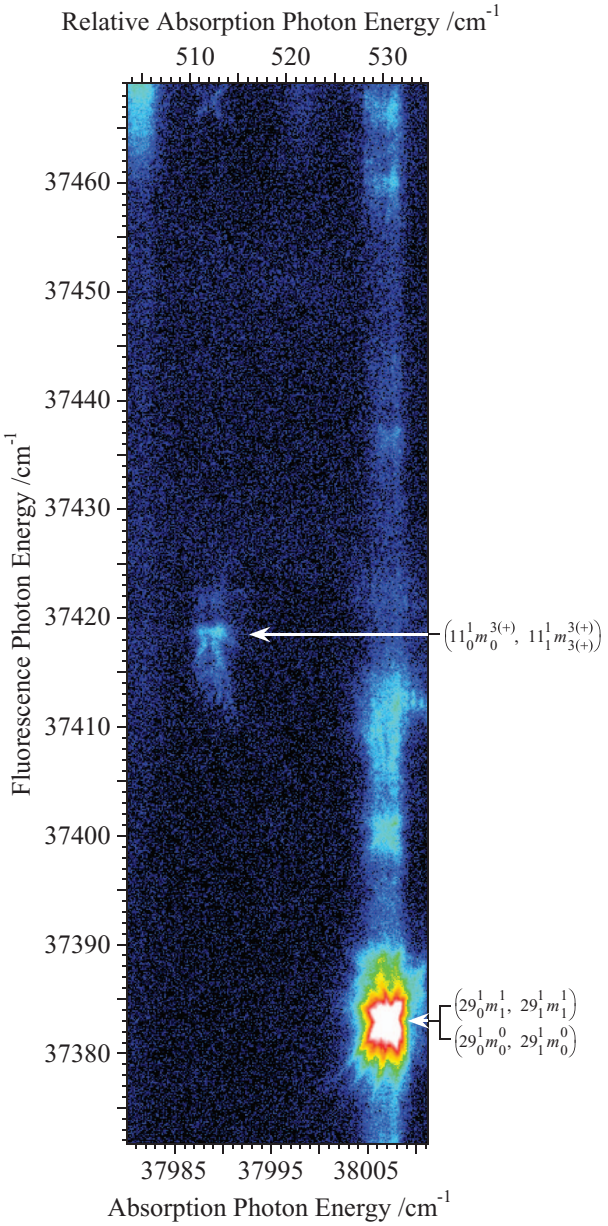

FIG. 7. The 2D-LIF spectral image obtained by scanning the laser over the region where the absorption features $14_0^2 m_0^{3(+)}$, $11_0^1 m_0^{3(+)}$, and $19_0^1 20_0^1 m_0^{3(+)}$ are expected while monitoring emission from the excited states to $11_1 m_{3(+)}$. This reveals the 11^1 component of the Femi resonance at $m' = 3a_1''$. Only one band is seen, indicating that the resonance is so weak that it is unobserved here. The feature at the top left hand corner of the figure is associated with excitation of the $\overline{29_0^1}$ band of toluene-Ar (Ref. 48), which dissociates prior to emission, populating rotational states of the toluene 0^0 level (see also Fig. 3(b)). The vertical series of features on the right hand side of the figure is associated with emission following excitation of 29_0^1. The horizontal axis at the top of the figure shows the displacement relative to the m_0^0 band at 37 476.6 cm^{-1} (Ref. 26).

on the generality of the effect and its consequences for time-resolved IVR experiments.

A. "Zero-order" states and coupling strengths

We first determine the "zero-order" states and their coupling strengths from the relative intensities and band separations (Tables III and IV). Since an analysis of this local resonance involves only $14^2 - 11^1 - 19^1 20^1$ coupling it ignores any longer range effects. Thus, the term "zero-order" in this context refers to a set of prediagonalised states where the only coupling not accounted for is the $14^2 - 11^1 - 19^1 20^1$ Fermi resonance.

In principle, the terms to be extracted from the analysis of the resonance are the energies of the three zero-order states, i.e., $E(14^2)$, $E(11^1)$, and $E(19^1 20^1)$ and the coupling terms between each of them, $V(11^1 - 14^2)$, $V(11^1 - 19^1 20^1)$, and $V(14^2 - 19^1 20^1)$. The coupling terms $V(11^1 - 14^2)$ and $V(11^1 - 19^1 20^1)$ are third order anharmonic terms, while

TABLE III. The relative intensities extracted from the 2D-LIF images shown in Figs. 4–6. The values determined from the calculated eigenvectors (Table VI) are shown for comparison.

Source	Terminating level in emission	Perturbed S_1 level excited		
Experiment[a]		$14^2m^0/14^2m^1$	$11^1m^0/11^1m^1$	$19^120^1m^0/19^120^1m^1$
	$11_1m_0/11_1m_1$	0.032/0.015	1.00	0.58/0.56
	$19_120_1m_0/19_120_1m_1$	Not observed	1.00	1.11
	$14_2m_0/14_2m_1$	1.36	1.00	0.15
Eigenvectors[b]		14^2m^0	11^1m^0	$19^120^1m^0$
This work	11_1m_0	0.032	1.00	0.58
	$19_120_1m_0$	0.005	1.00	1.15
	14_2m_0	1.78	1.00	0.11
		14^2m^1	11^1m^1	$19^120^1m^1$
	11_1m_1	0.015	1.00	0.56
	$19_120_1m_1$	0.002	1.00	1.09
	14_2m_1	1.89	1.00	0.14
		$14^2m^0/14^2m^1$	$11^1m^0/11^1m^1$	$19^120^1m^0/19^120^1m^1$
Davies and Reid [c]	$11_1m_0/11_1m_1$	0.001	1.00	0.78
	$19_120_1m_0/19_120_1m_1$	0.009	1.00	1.22
	$14_2m_0/14_2m_1$	0.34	1.00	0.12

[a]In emission to 19_120_1 and 14_2 the m_0^0 and m_1^1 transitions could not be separated. The values given for those terminating states are the total of the $m = 0$ and $m = 1$ contributions.
[b]The relative intensities depend on the oscillator strengths of both the excitation and emission steps. These can be calculated from the eigenvectors for the Fermi resonance states (see Table VI).
[c](Reference 7.) A single set of eigenvectors was provided incorporating both $m = 0$ and $m = 1$, and hence there is a single set of predicted relative intensities applying to both m states.

$V(14^2-19^120^1)$ is fourth order. Thus, $V(11^1-14^2)$ and $V(11^1-19^120^1)$ are expected to be an order of magnitude or so larger than $V(14^2–19^120^1)$.[50] For this reason we introduce the approximation that $V(14^2-19^120^1)$ is zero. With this approximation the coupling involves a bright state, 11^1, coupling to two dark states, 14^2 and 19^120^1, which do not interact. This situation can be analysed using a Green's function deconvolution method.[51]

The zero-order energies and coupling matrix elements extracted from the deconvolution for $m = 0$ and $m = 1$ are given in Table V. An energy level diagram of the observed and deperturbed states is shown in Fig. 8. The deconvolution is based on the energies and relative intensities extracted from Fig. 4 and shown in Tables III and IV. The relative intensities used in the deconvolution are the square root of the relative intensities seen in the 2D-LIF spectral images for the reasons discussed in Sec. III D 2. We reiterate that these extracted energies and coupling terms are "pre-diagonalised" and include any longer range perturbations that could shift their energy.

The key feature to emerge from the deconvolution is that the energy separations of the $m = 0$ and $m = 1$ "zero-order" states are different while their coupling terms are similar. This shows, as expected, that the mechanism coupling these states is not m-dependent and that the difference in spacing between

TABLE IV. The energy separations of the molecular eigenstates observed for the $m = 0$ and $m = 1$ levels of the $14^2-11^1-19^120^1$ resonance. The values determined from quantum beat experiments are also shown.

Perturbed states	Separation (cm^{-1})	
	This work	Davies *et al.*[a]
$14^2m^0-11^1m^0$	4.82	4.92
$11^1m^0-19^120^1m^0$	5.34	5.49
$14^2m^1-11^1m^1$	5.49	5.70
$11^1m^1-19^120^1m^1$	4.96	5.14

[a]Reference 7.

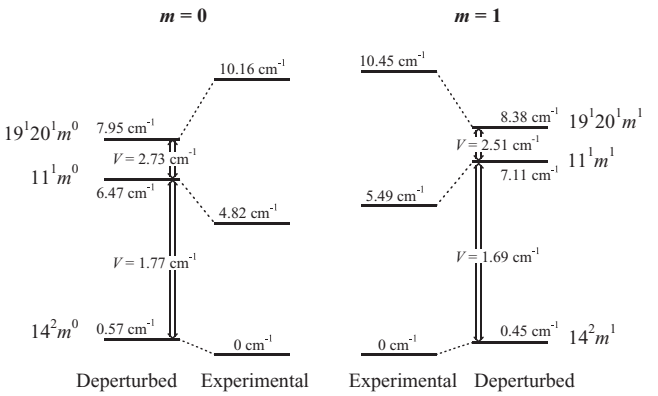

FIG. 8. An energy level diagram showing the relative energies of the $14^2-11^1-19^120^1$ Fermi resonance coupled states at $m = 0$ and $m = 1$ and the energies of the "zero-order" states obtained by deperturbing the local Fermi resonance as discussed in the text. The obtained coupling matrix elements, V, coupling the "zero-order" states are given in the diagram. The energy of the perturbed 14^2m^1 level is calculated to be 5.31 cm^{-1} above the perturbed 14^2m^0 level.

the eigenstates at $m = 0$ and $m = 1$ has its origin in differences in the separation of the zero-order states at these two m values. Variations in the torsional barrier height, V_6, and rotational constant for methyl internal rotation, F, with vibrational state could cause small changes in the $m = 0$ and $m = 1$ "zero-order" states but cannot account for the magnitude of the differences observed. This points to longer range interactions perturbing these "zero-order" states. The coupling terms, while very similar, are not identical, which is also consistent with longer range interactions causing the "zero-order" states to be slightly different mixtures of basis states at $m = 0$ and 1. Clearly, in the case of $m = 3a_1''$ the relative energies of the "zero-order" states are significantly different: their separation must be much larger since the resonance is no longer observed.

To explore the mechanism responsible for this m-dependent, long range perturbation we will examine in Sec. IV C the 11_1 region in S_0 where the separation of the $m = 0$ and 1 levels is larger than expected. This change in the m state energies for 11_1 is analogous to the different shifts seen for the $m = 0$ and 1 states in the $14^2-11^1-19^120^1$ Fermi resonance. Before doing this, we compare the results of our spectral analysis of the Fermi resonance with those reported by Davies *et al.*[7]

B. Comparison with quantum beat data analysis

Davies *et al.* have reported the separations between the molecular states for the $m = 0$ and 1 states of the $14^2-11^1-19^120^1$ Fermi resonance, obtained from analysis of time resolved, quantum beat experiments.[7] Our results are compared with theirs in Table IV. There is excellent agreement between the two sets of data, although there is a consistent trend for our values to be ~2%–4% below those reported by Davies *et al.* We are unsure of the reason for this difference.

Davies *et al.* were also able to determine the eigenvector matrix, which provides the coefficients for the molecular eigenstates expressed as linear combinations of the zero-order states, assuming the local Fermi resonance to be the only perturbation. Our analysis also enables these coefficients to be extracted by diagonalising the coupling matrix using the zero-order energies and coupling terms shown in Table V. They are shown in Table VI. In spite of the slightly different zero-order spacings and coupling matrix elements for $m = 0$ and 1, we find the two sets of eigenvectors to be almost identical. Comparing our eigenvectors with those of Davies *et al.* reveals quite good agreement in most cases. The primary difference is that in our case the perturbed 14^2 state has a reduced 19^120^1 component and an increased 11^1 component compared with the values determined by Davies *et al.* The calculated relative intensities for each of the Fermi triad emitting to 14_2, 11_1, and 19_120_1 are shown with our experimental values in Table III. Because the relative intensities depend on the coefficients of the corresponding S_1 states in the linear expansions, this comparison highlights the accuracy of the calculated coefficients. The bands most sensitive to the eigenvector coefficients are those from the Fermi triad that terminate in 14_2. The eigenvectors of Davies *et al.* underestimate the intensity of emission to 14_2 from the perturbed 14^2 level compared with emission from the perturbed 11^1 level. The experimental ratio is 1.36. Davies' eigenvectors predict a value of 0.34, i.e., 25% of that observed. Our eigenvectors predict values of 1.78 ($m = 0$) and 1.89 ($m = 1$), some 30%–40% larger than observed. The calculated ratios depend on products involving three of the eigenvector coefficients so we regard this as a quite acceptable level of agreement. In principle, one could improve the zero-order energies and coupling terms through an iterative procedure involving comparison with the observed intensities for the transitions terminating in the three states 14_2, 11_1, and 19_120_1; however, this would not change the overall picture or conclusions drawn.

TABLE V. The results of the deconvolution for $m = 0$ and $m = 1$ levels of the $14^2-11^1-19^120^1$ resonance.[a]

Zero-order states	Energy gap (cm^{-1})	Coupling strength (cm^{-1})
$14^2m^0-11^1m^0$	5.90	1.77
$11^1m^0-19^120^1m^0$	1.48	2.73
$14^2m^1-11^1m^1$	6.66	1.69
$11^1m^1-19^120^1m^1$	1.27	2.51

[a]The deconvolution is based on the energies given in Table IV and the relative intensities for emission to 11_1 given in Table III.

TABLE VI. The eigenvector matrices determined in this study and that determined by Davies *et al.* (Ref. 7). The eigenvector matrix provides the coefficients for the molecular eigenstates expressed as linear combinations of the zero-order states, assuming the local Fermi resonance to be the only perturbation.

m	Perturbed state	14^2 Coefficient	11^1 Coefficient	19^120^1 Coefficient
		This work		
0	14^2	−0.963	−0.250	0.099
	11^1	0.255	−0.728	0.636
	19^120^1	−0.087	0.638	0.765
1	14^2	−0.964	−0.245	0.107
	11^1	0.256	−0.732	0.632
	19^120^1	−0.077	0.636	0.768
		Davies *et al.*[a]		
0,1	14^2	−0.941	0.141	0.307
	11^1	0.316	0.721	0.616
	19^120^1	0.118	0.678	−0.725

[a]A single set of eigenvectors was reported incorporating both $m = 0$ and $m = 1$ (Ref. 7).

C. Torsion-vibration coupling involving 11_1: Long range, *m*-dependent perturbations

As discussed in Sec. III D 2, an unexpected doubling of the Fermi resonance features along the dispersed fluorescence axis is observed for transitions terminating in 11_1. It is most clearly evident in the $(11_0^1,11_1^1)$ case and is associated with a significant increase in the separation between the associated m_0^0 and m_1^1 transitions and a reversing of their energy ordering. By considering the absorption and emission energies for these features, it can be deduced that these changes are associated with a decrease of 1.8 cm^{-1} in the separation between the $m = 0$ and $m = 1$ levels for 11_1 compared with 0_0. This is a 34% decrease and cannot be explained by vibrationally

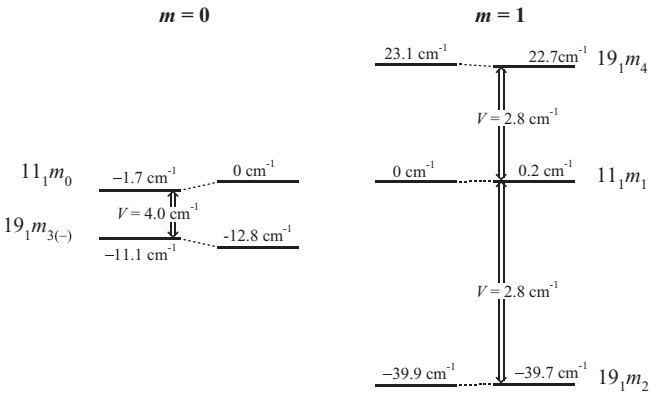

FIG. 9. An energy level diagram showing the relative energies of the 11_1-19_1 torsion-vibration coupled states and the energies of the "zero-order" states obtained by deperturbing the coupling as discussed in the text. The obtained coupling matrix elements, V, are given in the diagram.

induced changes in F or V_6. We show that the change is due to torsion-vibration coupling[6,37] that produces m-dependent energy shifts in the 11_1 m levels.

There are comparatively few well documented examples where torsion-vibration coupling has been analysed to extract coupling matrix elements in toluene derivatives[8,37–39] and the m-dependence of the selection rules do not appear to be explicitly developed for the toluene situation. Consequently, we have summarised the key points in Appendix B.

The low vibrational state density means that there are very few candidates for torsion-vibration coupling to 11_1. Figure 4 reveals evidence that torsion-rotation coupling between 11_1 and 19_1 is occurring, as observed by the presence of the otherwise forbidden emission features $19_1^1 20_0^1 m_{3(-)}^0$, $11_0^1 19_1^0 m_{3(-)}^0$, and $11_0^1 19_1^0 m_4^1$. The image is consistent with the couplings $11_1 m_0 - 19_1 m_{3(-)}$ and $11_1 m_1 - 19_1 m_4$ although, as we discuss further below, the relative intensities change in unexpected ways.

We now consider the 11_1-19_1 torsion-vibration coupling in detail. The $11_1 m_0$ level couples to $19_1 m_{3(-)}$ with a coupling matrix element $\sqrt{2}V$, while $11_1 m_1$ couples to both $19_1 m_2$ and $19_1 m_4$ with a coupling matrix element V (see Appendix B). From the calculated m_2-m_4 separation (Table II), the observed separations between the $11_1 m_0$ and $19_1 m_{3(-)}$ levels and between the $11_1 m_1$ and $19_1 m_4$ levels, and the observed change in the m_0-m_1 separation for 11_1, the coupling scheme shown in Fig. 9 has been deduced. A coupling matrix element of 2.8 cm^{-1} is determined, which is a low value by comparison with the torsion-vibration coupling terms observed spectroscopically in substituted toluenes.[6,37] We note, however, that the previously determined values all involve a linear, rather than quadratic, Q term, and linear terms are expected to generally be larger.[52] There are two other potential couplings that can shift $11_1 m_1$ to lower energy. These involve the states $14_1 m_5$ ($\Delta E = 17$ cm^{-1}) and $20_2 m_5$ ($\Delta E = 42$ cm^{-1}). Both could also be influencing the $11_1 m_1$ energy and hence the coupling constant extracted for the 11_1-19_1 interaction should be regarded as an upper limit.

While Fig. 4 reveals features consistent with torsion-vibration coupling between 11_1 and 19_1, the relative intensities observed are unusual. The transitions to $19_1 m_{3(-)}$ from the perturbed $11^1 m^0$ and $19^1 20^1 m^0$ levels should have the same relative intensity as those from these levels to $11_1 m_0$, since it is expected that the $11_1 m_0$ component of the perturbed $19_1 m_{3(-)}$ level provides the oscillator strength. Similarly, transitions to $19_1 m_4$ from $11^1 m^1$ and $19^1 20^1 m^1$ should have the same relative intensity as those from these levels to $11_1 m_1$, since it is the $11_1 m_1$ component of the perturbed $19_1 m_4$ level that is expected to provide the oscillator strength. In neither case is this observed. Moreover, there is a switch in which is the more intense transition, that from 11^1 or $19^1 20^1$, in the $19_1 m_{3(-)}$ and $19_1 m_4$ cases, with the perturbed $19^1 20^1 m^1$ emission intensity to $19_1 m_1$ vanishingly small. Noting that the terminating levels are linear combinations of $11_1 m_0$ and $19_1 m_{3(-)}$ in one case and $11_1 m_1$ and $19_1 m_4$ in the other, these observations can only be explained if the transitions from $11^1 m^0$ and $19^1 20^1 m^0$ to $19_1 m_{3(-)}$ and from $11^1 m^1$ and $19^1 20^1 m^1$ to $19_1 m_4$ have oscillator strength and there is interference between this component of the transition and the one involving the transition to the $11_1 m_0$ or $11_1 m_1$ component. The transitions from $11^1 m^0$ and $19^1 20^1 m^0$ to $19_1 m_{3(-)}$ and from $11^1 m^1$ and $19^1 20^1 m^1$ to $19_1 m_4$ involve one quantum changes in non-totally symmetric modes and so are not allowed. The observations imply that in the excited electronic state there is mixing of $11^1 m^0$ and $19^1 20^1 m^0$ with $19^1 m^{3(-)}$ and $11^1 m^1$ and $19^1 20^1 m^1$ with $19^1 m^4$: this mixing would provide an allowed $19_1^1 m_{3(-)}^{3(-)}$ or $19_1^1 m_4^4$ component to the transition. Given that 11_1 and 19_1 are observed to couple via torsion-vibration coupling in S_0, the van der Waals interaction mechanism proposed by Moss *et al.*[6] would lead to them also coupling in S_1. We point out that the energy separations of the interacting states will be different in the two electronic states due to changes in both the vibrational frequencies and rotor energies. With the 11^1 and $19^1 20^1$ vibrations strongly mixed by Fermi resonance in S_1, both mixed levels can couple to 19^1 via the 11^1 component. Torsion-vibration coupling could also occur between m levels in 19^1 and $19^1 20^1$ via a Q_{20} sin 3ϕ term. Interestingly, this is a lower order coupling term and hence is potentially larger than that for the 11^1-19^1 coupling, which involves $Q_{11}Q_{19}$ sin 3ϕ (Ref. 52).

D. Torsion-vibration coupling and the $14^2-11^1-19^1 20^1$ Fermi resonance

We return to the $14^2-11^1-19^1 20^1$ Fermi resonance to consider the mechanism responsible for the changes to the relative positions of the "zero-order" states with m. The lesson from our analysis of 11_1 is that "long range" torsion-vibration coupling can change the energies of the states and that these changes depend on the m level involved. The source of the m dependence is the $\Delta m = \pm 3n$ ($n = 1, 2, \ldots$) coupling selection rule in combination with the rotor energies scaling approximately with m^2.

The S_1 vibrational frequencies are lower than those in S_0 and as a result the vibrational state density surrounding 11^1 is higher than for 11_1. Table VII shows those levels within ± 100 cm^{-1} of 11^1 with the correct symmetry to couple with 14^2, 11^1, and $19^1 20^1$ via a torsion-vibration mechanism. Interestingly, examination of Table VII indicates an additional effect at play to contribute to the m dependence of the shifts

TABLE VII. The rotor-vibration levels calculated to lie within ±100 cm^{-1} of 11^1m^0 and 11^1m^1 and possessing the correct symmetry to couple via a torsion-vibration mechanism.

	State	ΔE[b] (cm^{-1})	Coupling term	$\Delta\upsilon$[a]	Δm
11^1m^0	$19^1m^{3(-)}$	−98	$Q_{11}Q_{19}\sin 3\alpha$	2	3
	$30^1m^{3(+)}$	−72	$Q_{11}Q_{30}\cos 3\alpha$	2	3
	$14^1m^{6(-)}$	−40	$Q_{11}Q_{14}\sin 6\alpha$	2	6
	$14^120^1m^{3(+)}$	−19	$Q_{11}Q_{14}Q_{20}\cos 3\alpha$	3	3
	$18^1m^{3(-)}$	14	$Q_{11}Q_{18}\sin 3\alpha$	2	3
	$20^2m^{6(+)}$	47	$Q_{11}Q_{20}^2\cos 6\alpha$	3	6
	$20^3m^{3(-)}$	53	$Q_{11}Q_{20}^3\sin 3\alpha$	4	3
11^1m^1	19^1m^4	−58	$Q_{11}Q_{19}\sin 3\alpha$	2	3
	$14^120^1m^2$	−58	$Q_{11}Q_{14}Q_{20}\cos 3\alpha$	3	3
	30^1m^4	−46	$Q_{11}Q_{30}\cos 3\alpha$	2	3
	20^2m^5	−17	$Q_{11}Q_{20}^2\cos 6\alpha$	3	6
	18^1m^2	−11	$Q_{11}Q_{18}\sin 3\alpha$	2	3
	$14^120^1m^4$	7	$Q_{11}Q_{14}Q_{20}\cos 3\alpha$	3	3
	14^1m^7	24	$Q_{11}Q_{14}\sin 6\alpha$	2	6
	20^3m^2	28	$Q_{11}Q_{20}^3\sin 3\alpha$	4	3
	18^1m^4	54	$Q_{11}Q_{18}\sin 3\alpha$	2	3
	20^3m^4	93	$Q_{11}Q_{20}^3\sin 3\alpha$	4	3

[a]$\Delta\upsilon$ denotes the total change in vibrational quantum number between 11^1 and the other vibrational state.

[b]The S_1 frequencies used for this calculation are those provided by Hickman *et al.* (Ref. 15) except for 18^1 which is taken from the REMPI study by Gardner *et al.* (Ref. 27).

arising from torsion-vibration coupling. It can be seen that the number of states in the ±100 cm^{-1} window that can couple is larger for $m = 1$ than for $m = 0$ because $m = 1$ can couple via, for example, $\Delta m = \pm 3$ to the $m = 2$ and 4 levels of another vibration, whereas $m = 0$ can only couple to $m = 3$ (see Appendix B).

The 19^1 level, which is listed in Table VII, was identified as one of the coupled states in Sec. IV C. However, this coupling cannot explain the different "zero-order" separations between the Fermi resonance coupled states at $m = 0$ and $m = 1$ because the shifts induced by 19^1 are almost the same for $m = 0$ and 1. This occurs because, although the separation between the coupled states reduces from ∼100 cm^{-1} for the $m = 0$ case to ∼60 cm^{-1} for the $m = 1$ case, the coupling for $m = 0-3a_1''$ is larger than for $m = 1-4$ by a factor of $\sqrt{2}$ (see Appendix B). The energy shifts, which scale as $V^2/\Delta E$, are almost the same in the two cases.

The key to unlocking the identity of the state responsible for the torsion-rotation coupling that alters the separation of the Fermi resonance coupled states at $m = 0$ and $m = 1$ was provided by the REMPI spectrum of Gardner *et al.* (see Fig. 10), measured as part of a zero kinetic energy (ZEKE) photoelectron study.[27] The REMPI spectrum reveals bands that do not appear in the 2D-LIF spectra because absorption bands that lead to emission outside of the narrow fluorescence region observed are "dark" in the 2D-LIF experiment. Gardner *et al.* suggested that a weak band ∼15 cm^{-1} to higher energy of the 11_0^1 band is the $18_0^1m_0^{3(-)}$ transition on the basis that $18^1m^{3(-)}$ is of the correct symmetry to gain intensity through torsion-vibration coupling to 11^1m^0 (see Table VII). (This feature is labeled B and D in Fig. 10 consistent with the nomenclature used by Gardner *et al.* in their analysis.) From Table VII, this requires that the $\mathcal{M}_{18}$ S_1 frequency be revised

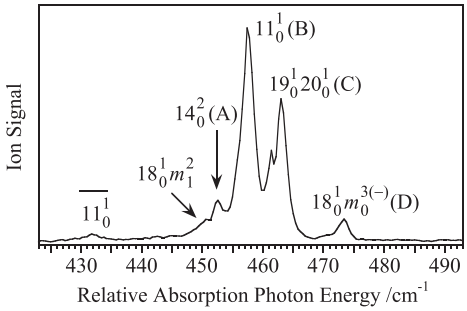

FIG. 10. REMPI spectrum in the region of the $14^2-11^1-19^120^1$ Fermi triad provided by Gardner *et al.* (Ref. 27).

upwards by ∼10 cm^{-1}, which is not unreasonable given that it was deduced from a deperturbed combination band assuming no anharmonicity.[15]

In view of this suggestion, we have explored the implications of torsion-vibration coupling involving 11^1 and 18^1. This term is expected to be significantly larger than the coupling of 18^1 to either 19^120^1 or 14^2 since it involves $\Delta\upsilon = 2$ while they both involve $\Delta\upsilon = 3$.[52] Consequently, we assume that the dominant coupling involves 11^1 and 18^1. The resulting coupling scheme, including the anharmonic coupling terms determined in Sec. IV A, is shown in Fig. 11. On the basis of the energy shifts observed for 11^1m^0 and 11^1m^1 we estimate a torsion-vibration coupling constant of 1.9 cm^{-1}. As discussed in Sec. IV C, this is a modest value.

The torsion-vibration coupling scheme shown in Fig. 11 can be tested through the predicted intensities of the $18_0^1m_1^2$ and $18_0^1m_0^{3(-)}$ transitions relative to the $11_0^1m_1^1$ and $11_0^1m_0^0$ transitions, assuming the former to gain oscillator strength solely from the 11^1 components of the perturbed states. $18_0^1m_0^{3(-)}$ is predicted to have 3.6% of the $11_0^1m_0^0$ transition intensity, while $18_0^1m_1^2$ is predicted to have 2.9% of the $11_0^1m_1^1$ intensity. Comparing these predictions with the values observed in the REMPI spectrum is complicated because the 11^1 intensity is spread across three bands by the Fermi resonance and because of the overlap of the m_0^0 and m_1^1 transitions associated with each of them. By assuming that the intensity in the Fermi resonance bands is evenly split between the m_0^0 and m_1^1 transitions, and summing the intensity to each of the three components to extract the total 11_0^1 transition intensity, we estimate the $18_0^1m_0^{3(-)}$ intensity observed to be ∼3.3% of the $11_0^1m_0^0$ transition, very close to the expected value of 3.6%. Importantly, for this assignment to be correct we also predict that a slightly weaker band, $18_0^1m_1^2$, should be seen in the spectrum ∼10 cm^{-1} below the 11_0^1 band. Examination of Fig. 10 shows that the 14_0^2 band, labeled B and A by Gardner *et al.*, appears on top of a broad feature that begins ∼10 cm^{-1} below 11_0^1. A broad feature is expected for a m_1^2 band (see, for example, Fig. 1). We suggest that the broad feature beginning to the low energy side of 14_0^2 and underlying this band is the $18_0^1m_1^2$ band that has gained intensity due to torsion-vibration coupling with 11^1m^1. Its position is a few wavenumbers higher than expected, but given that it is overlapped with 14_0^2, determining the band position is difficult. While the overlap of these bands makes extracting the $18_0^1m_1^2$ relative

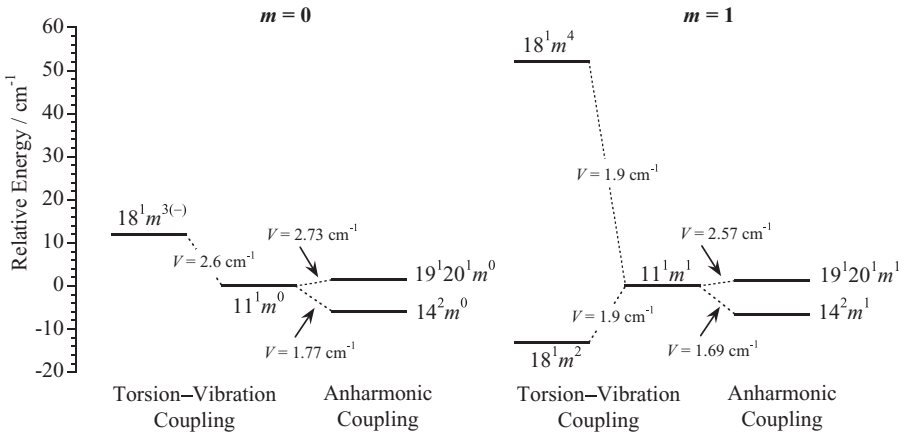

FIG. 11. An energy level diagram showing the coupling scheme deduced for the anharmonic and torsion-vibration couplings influencing the $14^2-11^1-19^120^1$ Fermi triad and responsible for its m dependence.

intensity problematic, it appears to be consistent with the predicted value.

The torsion-vibration coupling of rotor levels built on 18^1 with those of 11^1 provides an explanation for the m-dependent energy differences observed in the $14^2-11^1-19^120^1$ Fermi resonance at $m = 0$ and $m = 1$. Accounting for this coupling leads to the prediction of a weak $18^1_0m^2_1$ band near 14^2_0 and such a feature is observed. The addition of a second torsion-vibration coupling involving 19^1 is required to explain the relative intensities seen in dispersed fluorescence from the Fermi resonance coupled states to rotor levels of 19_1 in S_0. While we cannot rule out the involvement of other states, the 2D-LIF spectral images and REMPI spectrum can be explained by these coupling pathways. We note that, if these are the sole coupling pathways influencing the $14^2-11^1-19^120^1$ Fermi resonance, in principle, it should be possible to deduce a complete coupling matrix for the $m = 1$ and $m = 0$ levels for which both the anharmonic coupling terms and zero-order $14^2-11^1-19^120^1$ separations are the same: the differences deduced in the de-perturbation process (see Figs. 8 and 11) would arise as a consequence of the energy and mixing coefficients being different at $m = 0$ and $m = 1$ due to the different torsion-vibration couplings. This has not been pursued since it does not add further insight beyond the sequential analyses already reported.

Finally, we consider the case of $m = 3a''_1$. A single band is observed in the 2D-LIF image, with no evidence for the Fermi resonance occurring at this m level. Given that at $m = 0$ and 1 the Fermi resonance coupling matrix element is $\sim$2.6 cm^{-1} and the separation between the 11^1 and 19^120^1 "zero-order" states is $\sim$1.4 cm^{-1}, large shifts in the $m = 3a''_1$ "zero-order" states are required for the interaction to be unobserved. It is important in this context to note that the experiment does amplify intensity differences through the absorption/emission process involved in 2D-LIF spectral images. Nevertheless, no trace is seen of coupled states at $m = 3a''_1$ in Fig. 7. Examination of the position of the $11^1_0m^{3(+)}_0$ absorption feature shows it to be 54.8 cm^{-1} above the position of the deperturbed $11^1_0m^0_0$ band. In comparison, the $0^0_0m^{3(+)}_0-0^0_0m^0_0$ separation is observed to be 54.2 cm^{-1}. This indicates that the $11^1m^{3(+)}$ level is little shifted, suggesting that the $19^120^1m^{3(+)}$ level has been substantially perturbed. Because the mechanism leading to this shift is m dependent, it involves a torsion-vibration coupling. There are several states with the correct symmetry to couple to $19^120^1m^{3(+)}$ nearby. Interestingly, the closest state, and the one involving the lowest order term, is $19^1m^{6(+)}$. If this state is involved we might expect that $11^1m^{3(+)}$ would also be perturbed, yet this does not appear to be occurring. This implies that, if $19^1m^{6(+)}$ is the state responsible for perturbing $19^120^1m^{3(+)}$, the Q_{20} sin 3ϕ term is significantly larger than the $Q_{11}Q_{19}$ sin 3ϕ term. Such a situation is consistent with the coupling model proposed by Parmenter[6] for which coupling terms linear in Q are largest.[52]

E. The long range influence of torsion-vibration coupling

We here consider how important and universal the m-dependent energy perturbations observed in toluene are likely to be. In considering this issue it is useful to review the magnitude of torsion-vibration interactions where such resonances have been observed and analysed. Weisshaar and coworkers[37] have analysed several local torsion-vibration resonances in substituted toluenes. The observed coupling terms were of the form Q sin 3ϕ or Q cos 3ϕ, i.e., they involved a $\Delta m = 3$ coupling with a change of ±1 in a single vibrational mode. The coupling terms extracted range from 3.5 to 14.8 cm^{-1}, with an average value of 8 cm^{-1}. A 0.5 cm^{-1} shift in an m state arising from an 8 cm^{-1} coupling occurs with a ΔE of $\sim$130 cm^{-1}. This illustrates that for substituted toluenes it is likely to be the norm for states involved in a local interaction such as a Fermi resonance to also be coupled via torsion-vibration coupling to states some distance removed in energy and that this interaction can differentially move m states around by small amounts. Consequently, we suggest that the effect seen by Reid's group, whereby $m = 0$ and 1 eigenstates have different spacings,[7,8,14] is likely to be the usual situation.

In this context, we have earlier shown in Fig. 2 a series of m-resolved rotational contours for the main bands seen in the 2D-LIF images of Figs. 1 and 3. These illustrate the range of shifts seen between the m^0_0 and m^1_1 transitions associated with

various vibrational levels. None of the states observed has the same spacing as the 0_0^0 band. While this is not surprising in view of the fact that several of the bands are associated with the Fermi resonance where this was expected, a change is also clearly seen for 29_0^1, which is not part of the Fermi resonance. These shifts appear to be pervasive.

In considering how wide ranging we anticipate the effects of torsion-vibration coupling to be, understanding the mechanism(s) responsible for it and predicting its magnitude are central. Two mechanisms have been proposed. Moss *et al.* put forward a model based on through-space, van der Waals interactions between atoms of the ring and methyl rotor.[6] Rotation of the methyl rotor modulates the force on ring atoms because the van der Waals interaction is a function of the position of the methyl hydrogens. This model, which formed the basis of Martens and Reinhardt's theoretical modeling of IVR behavior in *p*-fluorotoluene,[52] is universal in that van der Waals forces between the methyl hydrogens and other atoms will always be present and modulated by methyl rotation. However, the data provided by Borst and Pratt's high precision rotational analysis allowed those authors to obtain detailed insight into the modulation of the ring by the methyl rotation and this provided an alternative picture.[26] While acknowledging that the van der Waals mechanism may play a role, Borst and Pratt showed that their data provided direct evidence for the torsional motion coupling ring vibrations based on an electronic effect. In essence, the rotor motion modulates the electronic structure, which leads to changes in the ring geometry, giving a direct coupling between rotor motion and ring vibrations. While beyond the scope of the present paper, it would be interesting to explore the extent to which these methyl-modulated, electronically induced structural changes in the ring link particular vibrational modes and the magnitude of such effects. With several torsion-vibration coupling interactions exposed in the present work, there is an opportunity to calculate the magnitude of the coupling constants for both of the mechanisms to determine their relative contributions.

V. CONCLUSIONS

We have used 2D-LIF spectral imaging to investigate the m dependence of the $14^2-11^1-19^120^1$ Fermi resonance in S_1 toluene. Davies *et al.* showed through an analysis of their quantum beat data that the eigenstates have different energy spacings at $m = 0$ and 1 for this resonance.[7] The 2D-LIF technique has provided a means to dissect the interaction at each m level. An analysis of the 2D-LIF spectral images has provided the energy separations of the eigenstates and their relative intensities for individual m values, allowing the m-dependent interactions to be de-perturbed and the coupling matrix elements and zero-order energies to be extracted. Using these data the eigenstates could be expressed in terms of a linear sum of the zero-order states. The key outcome of this analysis is that the different energy separations observed for the eigenstates at $m = 0$ and $m = 1$ arise because the zero-order states themselves have a different spacing at these two m values. This happens because the zero-order states involved in the local resonance are themselves the result of longer range torsion-rotation coupling that moves the states by small amounts.

The long range torsion-vibration coupling was exemplified by examining the case of 11_1 in S_0. Shifts in the m states were observed in the case of 11_1 and we showed unambiguously that this arises through torsion-vibration coupling involving 19_1. The analysis of the 11_1 interactions showed how long range torsion-vibration coupling can change the energies of the states and, moreover, how these changes are m dependent. The m dependence arises primarily because of the $\Delta m = \pm 3n$ ($n = 1, 2, \ldots$) coupling selection rule in combination with the fact that the rotor energies scale approximately with m^2, which changes the ΔE for the interaction for each m. In addition, more states can couple for $m = 1$ than for $m = 0$. Analysis of the $14^2-11^1-19^120^1$ Fermi resonance indicates that torsion-vibration coupling of rotor levels built on 18^1 with those of 11^1 can explain the m-dependent energy differences observed. The addition of a second torsion-vibration coupling involving 19^1 is required to explain the relative intensities seen in dispersed fluorescence from the Fermi resonance coupled states to rotor levels built on 19_1 in S_0. The Fermi resonance is not observed at the $11^1m^{3(+)}$ level and this is most likely the result of $19^120^1m^{3(+)}$ being significantly shifted by torsion-vibration coupling involving an unidentified state.

Consideration of the magnitude of reported torsion-rotation coupling constants for substituted toluenes suggests that this effect is likely to be pervasive in these molecular systems. Thus, time resolved measurements of intramolecular vibrational energy redistribution are likely to find an m dependence to these measurements to be the common situation. This is consistent with such effects being observed in the systems so far studied by Reid's group.

ACKNOWLEDGMENTS

We acknowledge Flinders University for financial support and the support provided by the School of Chemical and Physical Sciences Electronic and Mechanical workshops. We thank Katharine Reid from The University of Nottingham for stimulating our interest in this problem. We also thank Timothy Wright and Adrian Gardner from The University of Nottingham for supplying their toluene REMPI data and an early copy of their paper. We enjoyed stimulating email discussions with Katharine Reid, Timothy Wright, and Adrian Gardner about many aspects of toluene spectroscopy.

APPENDIX A: TOLUENE VIBRATIONAL MODE NUMBERING

Several mode numbering schemes have been used for assigning the vibrations of toluene.[15,28–32] Wilson's scheme for benzene,[53] correlated to the vibrational modes of toluene, has been used predominantly although there are variations in the assignments to particular vibrational frequencies, as discussed by Hickman *et al.*[15] There is also the issue of how to handle the methyl vibrations in this situation. To overcome these issues Hickman *et al.*[15] proposed an alternative notation based

on the Mulliken scheme,[54] which is widely used in substituted aromatic spectroscopy.

The issue of mode numbering in monosubstituted benzenes has recently been examined afresh by Gardner and Wright.[33] These authors have proposed a consistent numbering scheme based on the atomic displacements occurring during vibration which, if widely adopted, has the potential to alleviate the confusion that currently exists. Gardner and Wright's scheme numbers the 30 normal modes and assigns their symmetries in the C_{2v} symmetry group. They have extended this numbering system to multi-atom substituents where the substituent is considered as a point mass. Toluene involves the addition of a methyl group to benzene and so it is necessary to also label its vibrations. Gardner and Wright did not discuss this issue in their study as it was focused on a systematic labeling for the aromatic modes. In addition to the mode numbering for the methyl vibrations, the addition of the methyl group adds the complication that the molecule can no longer be classified strictly as C_{2v}, although much of its spectroscopy can be understood within the constraints of that group. Toluene is properly assigned to the permutation-inversion group G_{12}. In order to assign the methyl modes or, more generally, the modes of a poly-atom mono-substituent, we suggest that they be treated as a separate set and labeled according to the Mulliken convention[54] in the appropriate symmetry group. This means labeling the modes in ascending order based on the vibrational frequencies arranged in descending order within each symmetry class, with the group's symmetry classes arranged in the usual order. In the toluene case, the methyl modes would be labeled in G_{12}, with the symmetry classes arranged in the order A_1', A_2', A_1'', and A_2''. Gardner and Wright have introduced the prefix $\mathcal{M}$ to indicate their mode numbering scheme. We suggest the use of a similar prefix, in this case an $\mathcal{S}$, to indicate the substituent modes. The vibrations of toluene in the G_{12} group have been discussed by Grošev *et al.*[55] Table I gives the S_0 vibrational frequencies and correlates the various mode numbering schemes that have been proposed. Note that a consequence of using Gardner and Wright's ordering of the substituted benzene modes is that they are not sequential in G_{12} because B_1 of C_{2v} correlates with A_2'' while B_2 correlates with A_1''.

Throughout this work we use the numbering scheme proposed by Gardner and Wright for the ring modes, as shown in Table I. For brevity, we omit the label $\mathcal{M}$ in identifying transitions and levels using the common convention of a mode number with a superscript/subscript to denote the number of vibrational quanta in the upper/lower state. For example, the transition $\mathcal{M}_{19}{}^{1}_{0}$ will be written 19^1_0. All of the vibrational modes studied here are ring modes and so involve the $\mathcal{M}$ identifier. Omission of $\mathcal{M}$ should thus not cause confusion with methyl modes.

APPENDIX B: TORSION-VIBRATION COUPLING

The coupling terms are products of a coupling constant, $V_{T\text{-}V}$, normal coordinate operators, Q, and torsion operators, $\cos(3n\phi)$ or $\sin(3n\phi)$, where $n = 1, 2\ldots$ (Refs. 6 and 37–39):

$$V_{T-V}\, Q_i\, Q_j \ldots \cos(3n\phi) \text{ or } V_{T-V}\, Q_i\, Q_j \ldots \sin(3n\phi).$$

The number of normal coordinate operators involved depends on the vibrational quantum differences between the two coupled states. For example, coupling between an m level in the state X^1 with a different m level in the state Y^1 would involve a $Q_X Q_Y$ term since there is a $\Delta\upsilon = 1$ change in each of ν_X and ν_Y. The product of the operators must transform as the totally symmetric representation, i.e.,

$$\Gamma_{Q_i} \otimes \Gamma_{Q_j} \otimes \cdots \otimes \Gamma_{\cos(3n\phi)} \supset A_1'',$$

in the case of toluene (and similarly for the $\sin(3n\phi)$ term). The coupling interaction is expected to decrease with increasing n and increasing power of Q.[52]

Approximating the vibrations as simple harmonic oscillators, the Q_i terms can be readily evaluated (see Appendix III of Ref. 56). Their value depends on the number of quanta in the vibrational modes coupled and the change in vibrational quanta, $\Delta\upsilon$, involved.

Using the $\exp(im\phi)$ basis functions for the rotor, the $\cos(3n\phi)$ and $\sin(3n\phi)$ terms lead to a $\Delta m = \pm 3n$, $n = 1, 2\ldots$ selection rule and a coupling term that is independent of m. However, these basis functions do not accurately describe the rotor levels, which are properly described by linear combinations of these functions. For most rotor levels in toluene the distinction is moot because the interaction term that mixes them depends on the barrier height, which is small, and an m state is well approximated by a single $\exp(im\phi)$ term. However, the $m = 3$ states are an exception and need to be considered in detail, since coupling from $m = 0$ levels can occur to $m = 3$ states.

Toluene has a six-fold torsion potential, which leads to the basis functions separated by $\Delta m = \pm 6$ being mixed. The basis functions have energies given by m^2F. The two $m = 3$ states, $3a_1''$ and $3a_2''$, arise from a direct interaction between the $m = +3$ and $m = -3$ basis functions. Since the $m = \pm 3$ basis functions are energetically degenerate, the rotor states are equal mixtures of the two basis functions and, in the case of toluene, are well-described by

$$|3a_1''\rangle = \frac{1}{\sqrt{2}}\left(|+3\rangle + |-3\rangle\right) \quad \text{and}$$

$$|3a_2''\rangle = \frac{1}{\sqrt{2}}\left(|+3\rangle - |-3\rangle\right).$$

This affects the value of the coupling term when one of these two states is involved, with it being $\sqrt{2}$ larger.

A further issue that needs to be examined is the effect of the $\Delta m = \pm 3n$ rule at low m, where states that do not appear to meet the selection rule can couple. Consider, for example, the situation for coupling involving an $m = 1$ level in the $n = 1$ case, i.e., $\Delta m = \pm 3$. The state labeled $m = 1$ is a degenerate level involving $m = +1$ and $m = -1$ states. (These correspond to the rotor spinning in opposite directions.) A $+3$ change in m from $m = -1$ couples $m = 2$, while a -3 change couples $m = -5$. Similarly, a $+3$ change in m from $m = +1$ couples $m = +5$, while a -3 change couples $m = -2$. An $m = 1$ level thus can couple to an $m = 2$ or $m = 5$ level, although it appears superficially that the $m = 1$ to $m = 2$ coupling is not allowed by the $\Delta m = \pm 3$ selection rule.

Finally, we note that the m dependence of the rotor energies leads to the effect of the coupling between, for example, the states $X_1 m_i$ and $Y_1 m_{i+3}$ being quite different to that between the states $X_1 m_{i+1}$ and $Y_1 m_{i+4}$. In first order perturbation terms, the energy shift of a level scales as $V^2/\Delta E$, where V is the coupling term and ΔE is the separation between the coupled states. While V is essentially the same in the two cases (except for the $i = 0$ case where it is $\sqrt{2}$ larger, as discussed above), the m dependence of the rotor energies changes ΔE substantially. The energy shifts associated with coupling between a particular pair of vibrational states are thus, in general, m dependent.

[1] C. S. Parmenter and B. M. Stone, J. Chem. Phys. **84**, 4710 (1986).
[2] Q. Ju, C. S. Parmenter, T. A. Stone, and Z. Q. Zhao, Isr. J. Chem. **37**, 379 (1997).
[3] R. J. Longfellow and C. S. Parmenter, J. Chem. Soc., Faraday Trans. 2 **84**, 1499 (1988).
[4] D. B. Moss and C. S. Parmenter, J. Chem. Phys. **98**, 6897 (1993).
[5] P. J. Timbers, C. S. Parmenter, and D. B. Moss, J. Chem. Phys. **100**, 1028 (1994).
[6] D. B. Moss, C. S. Parmenter, and G. E. Ewing, J. Chem. Phys. **86**, 51 (1987).
[7] J. A. Davies, A. M. Green, and K. L. Reid, Phys. Chem. Chem. Phys. **12**, 9872 (2010).
[8] J. A. Davies and K. L. Reid, J. Chem. Phys. **135**, 124305 (2011).
[9] J. A. Davies, K. L. Reid, M. Towrie, and P. Matousek, J. Chem. Phys. **117**, 9099 (2002).
[10] K. L. Reid, Int. Rev. Phys. Chem. **27**, 607 (2008).
[11] P. T. Whiteside, A. K. King, J. A. Davies, K. L. Reid, M. Towrie, and P. Matousek, J. Chem. Phys. **123**, 204317 (2005).
[12] C. J. Hammond, V. L. Ayles, D. E. Bergeron, K. L. Reid, and T. G. Wright, J. Chem. Phys. **125**, 124308 (2006).
[13] C. J. Hammond, K. L. Reid, and K. L. Ronayne, J. Chem. Phys. **124**, 201102 (2006).
[14] J. A. Davies and K. L. Reid, Phys. Rev. Lett. **109**, 193004 (2012).
[15] C. G. Hickman, J. R. Gascooke, and W. D. Lawrance, J. Chem. Phys. **104**, 4887 (1996).
[16] J. R. Gascooke, U. N. Alexander, and W. D. Lawrance, J. Chem. Phys. **134**, 184301 (2011).
[17] J. R. Gascooke, U. N. Alexander, and W. D. Lawrance, J. Chem. Phys. **136**, 134309 (2012).
[18] J. R. Gascooke and W. D. Lawrance, Chem. Phys. Lett. **555**, 38 (2013).
[19] J. A. Joester, M. Nakajima, N. J. Reilly, D. L. Kokkin, K. Nauta, S. H. Kable, and T. W. Schmidt, J. Chem. Phys. **127**, 214303 (2007).
[20] M. Nakajima, J. A. Joester, N. I. Page, N. J. Reilly, G. B. Bacskay, T. W. Schmidt, and S. H. Kable, J. Chem. Phys. **131**, 044301 (2009).
[21] N. J. Reilly, D. L. Kokkin, M. Nakajima, K. Nauta, S. H. Kable, and T. W. Schmidt, J. Am. Chem. Soc. **130**, 3137 (2008).
[22] N. J. Reilly, M. Nakajima, B. A. Gibson, T. W. Schmidt, and S. H. Kable, J. Chem. Phys. **130**, 144313 (2009).
[23] N. J. Reilly, M. Nakajima, T. P. Troy, N. Chalyavi, K. A. Duncan, K. Nauta, S. H. Kable, and T. W. Schmidt, J. Am. Chem. Soc. **131**, 13423 (2009).
[24] N. J. Reilly, T. W. Schmidt, and S. H. Kable, J. Phys. Chem. A **110**, 12355 (2006).
[25] T. P. Troy, M. Nakajima, N. Chalyavi, K. Nauta, S. H. Kable, and T. W. Schmidt, J. Phys. Chem. A **116**, 7906 (2012).
[26] D. R. Borst and D. W. Pratt, J. Chem. Phys. **113**, 3658 (2000).
[27] A. M. Gardner, A. M. Green, V. M. Tamé-Reyes, V. H. K. Wilton, and T. G. Wright, J. Chem. Phys. **138**, 134303 (2013).
[28] K. S. Pitzer and D. W. Scott, J. Am. Chem. Soc. **65**, 803 (1943).
[29] N. Fuson, C. Garrigou-Lagrange, and M. L. Josien, Spectrochim. Acta **16**, 106 (1960).
[30] G. Varsanyi, *Assignments for Vibrational Spectra of Seven Hundred Benzene Derivatives* (Wiley, New York, 1974).
[31] L. M. Sverdlov, M. A. Kovner, and E. P. Krainov, *Vibrational Spectra of Polyatomic Molecules* (Wiley, New York, 1973).
[32] M. Tasumi, T. Urano, and M. Nakata, J. Mol. Struct. **146**, 383 (1986).
[33] A. M. Gardner and T. G. Wright, J. Chem. Phys. **135**, 114305 (2011).
[34] L. H. Spangler, Annu. Rev. Phys. Chem. **48**, 481 (1997).
[35] S. H. Feldgus, M. J. Schroeder, R. A. Walker, W. K. Woo, and J. C. Weisshaar, Int. J. Mass Spectrom. Ion Process. **159**, 231 (1996).
[36] K. T. Lu and J. C. Weisshaar, J. Chem. Phys. **99**, 4247 (1993).
[37] E. C. Richard, R. A. Walker, and J. C. Weisshaar, J. Chem. Phys. **104**, 4451 (1996).
[38] R. A. Walker, E. C. Richard, K. T. Lu, and J. C. Weisshaar, J. Phys. Chem. **99**, 12422 (1995).
[39] R. A. Walker, E. C. Richard, and J. C. Weisshaar, J. Phys. Chem. **100**, 7333 (1996).
[40] P. J. Breen, J. A. Warren, E. R. Bernstein, and J. I. Seeman, J. Chem. Phys. **87**, 1917 (1987).
[41] V. Amir-Ebrahimi, A. Choplin, J. Demaison, and G. Roussy, J. Mol. Spectrosc. **89**, 42 (1981).
[42] W. A. Kreiner, H. D. Rudolph, and B. T. Tan, J. Mol. Spectrosc. **48**, 86 (1973).
[43] H. D. Rudolph, H. Dereizler, A. Jaeschke, and P. Wendling, Z. Naturforsch. A **22a**, 940 (1967).
[44] A. L. L. East, H. Liu, E. C. Lim, P. Jensen, I. Dechene, M. Z. Zgierski, W. Siebrand, and P. R. Bunker, J. Chem. Phys. **112**, 167 (2000).
[45] R. A. Walker, E. Richard, K. T. Lu, E. L. Sibert, and J. C. Weisshaar, J. Chem. Phys. **102**, 8718 (1995).
[46] H. Inoue, S. Sato, and K. Kimura, J. Electron Spectrosc. Relat. Phenom. **88–91**, 125 (1998).
[47] M. Mons, J. Le Calvé, F. Piuzzi, and I. Dimicoli, J. Chem. Phys. **92**, 2155 (1990).
[48] R. J. Doyle, E. S. J. Love, R. Da Campo, and S. R. Mackenzie, J. Chem. Phys. **122**, 194315 (2005).
[49] J. R. Gascooke and W. D. Lawrance, J. Chem. Phys. **138**, 084304 (2013).
[50] N. T. Whetton and W. D. Lawrance, J. Phys. Chem. **93**, 5377 (1989).
[51] W. D. Lawrance and A. E. W. Knight, J. Phys. Chem. **89**, 917 (1985).
[52] C. C. Martens and W. P. Reinhardt, J. Chem. Phys. **93**, 5621 (1990).
[53] E. B. Wilson, Phys. Rev. **45**, 706 (1934).
[54] R. S. Mulliken, J. Chem. Phys. **23**, 1997 (1955).
[55] V. M. Grosev, H. W. Schrotter, and J. Jonuscheit, J. Raman Spectrosc. **26**, 137 (1995).
[56] E. B. Wilson, J. C. Decius, and P. C. Cross, *Molecular Vibrations: The Theory of Infrared and Raman Vibrational Spectra* (Dover Publications Inc., New York, 1955).